

2005

Robustness of disturbance observer on a six-DOF dynamic system

Michael Sungmin Cho
San Jose State University

Follow this and additional works at: https://scholarworks.sjsu.edu/etd_theses

Recommended Citation

Cho, Michael Sungmin, "Robustness of disturbance observer on a six-DOF dynamic system" (2005). *Master's Theses*. 2750.
DOI: <https://doi.org/10.31979/etd.na43-rqh5>
https://scholarworks.sjsu.edu/etd_theses/2750

This Thesis is brought to you for free and open access by the Master's Theses and Graduate Research at SJSU ScholarWorks. It has been accepted for inclusion in Master's Theses by an authorized administrator of SJSU ScholarWorks. For more information, please contact scholarworks@sjsu.edu.

ROBUSTNESS OF DISTURBANCE OBSERVER
ON A SIX-DOF DYNAMIC SYSTEM

A Thesis

Presented to

The Faculty of the Department
of Mechanical and Aerospace Engineering
San Jose State University

In Partial Fulfillment

of the Requirements for the Degree

Master of Science

By

Michael Sungmin Cho

August 2005

UMI Number: 1429413

INFORMATION TO USERS

The quality of this reproduction is dependent upon the quality of the copy submitted. Broken or indistinct print, colored or poor quality illustrations and photographs, print bleed-through, substandard margins, and improper alignment can adversely affect reproduction.

In the unlikely event that the author did not send a complete manuscript and there are missing pages, these will be noted. Also, if unauthorized copyright material had to be removed, a note will indicate the deletion.

UMI[®]

UMI Microform 1429413

Copyright 2006 by ProQuest Information and Learning Company.

All rights reserved. This microform edition is protected against unauthorized copying under Title 17, United States Code.

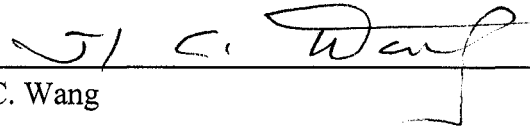
ProQuest Information and Learning Company
300 North Zeeb Road
P.O. Box 1346
Ann Arbor, MI 48106-1346

© 2005

Michael Sungmin Cho

ALL RIGHTS RESERVED

APPROVED FOR THE DEPARTMENT OF
MECHANICAL AND AEROSPACE ENGINEERING



Dr. Ji C. Wang



Dr. Fred Barez



Dr. Peter Reimer, Applied Materials

APPROVED FOR THE UNIVERSITY



ABSTRACT

ROBUSTNESS OF DISTURBANCE OBSERVER ON A SIX-DOF DYNAMIC SYSTEM

by Michael Sungmin Cho

This thesis addresses the challenges of the modern control algorithm faced with the requirements of high resolution in high speed operations. A multiple axis disturbance observer theory was developed on a six axis mathematical model to simulate the control algorithm generated from the fundamental theory of the disturbance observer.

The theory of the disturbance observer with the Computed Torque Control is applied to a multi-electron beam stage requiring nanometer accuracy, a mathematical model of the stage was derived using Euler's method, then the simulations using Matlab was done to verify the performance of the disturbance observer. This research has validated the performance of the disturbance observer in multi axis dynamic system where high speed output with nanometer accuracy is required.

ACKNOWLEDGEMENT

This thesis was completed with the guidance and patience of my advisor, Professor J.I. Wang of San Jose State University, Mechanical Engineering Department. The basis for the thesis was conceived during the 1999 project for the Ion Diagnostics' Multi Beam Stage Control of which this thesis' hardware specification was determined.

Professor Wang created the foundation of the stage control while detailed hardware design was furnished by Leonard Sharpless and Brian Alamo under the supervision of Dr. Gerry Andeen. Dr. Shin Il Wu provided the fundamentals in control engineering and Prof. Addis Tesfaye guided me in the mechatronics and hands-on aspect of control engineering.

My sincere appreciation to all those who patiently awaited the completion of this paper and supported me in various ways, especially Prof. Barez of San Jose State University, and Peter Reimer of Applied Materials.

TABLE OF CONTENTS

Introduction	1
Stage Design by Ion Diagnostics.....	4
Dynamic Mathematical Model of the Stage	10
External Forces and Moments Acting on the Stage	13
Methodology.....	18
Disturbance Observer Theory	21
State Space Dynamic Equations	28
Trajectory Generation.....	30
Simulation Analysis of the Computed Torque Controller	34
Simulation 1: Computed Torque Control with Zero Disturbance.....	36
Simulation 2: Large Disturbance on Computed Torque Control	38
Simulation 3: Disturbance Observer on Computed Torque Control ...	41
Conclusion.....	46
References.....	48
Appendix 1: Values and Definition of Variables	49
Appendix 2: Dynamic Equations of Motion Derivation	50

LIST OF FIGURES

Figure	Description	Page
Fig. 1	Stage Schematic	6
Fig. 2	Free Body Diagram of the Stage	7
Fig. 3	Stage Dimensions	9
Fig. 4	Euler's EOM Coordinate Systems	10
Fig. 5	Block Diagram of Compute Torque Control	18
Fig. 6	Block Diagram of Disturbance Observer	21
Fig. 7	Bode Plot of Q filters	24
Fig. 8	Block Diagram of Disturbance Observer w/ Filter	25
Fig. 9	Simulation Diagram with Double Integrator	26
Fig. 10	Simulation Output of Double Integrator	27
Fig. 11	Raster Trajectory	30
Fig. 12	Trajectory of Acceleration by LFPB	30
Fig. 13	Trajectory of LFPB	31
Fig. 14	Sinusoidal Position & Velocity Profile	32
Fig. 15	Sinusoidal Torque Profile	33
Fig. 16	Simulink Design of Computed Torque Control	36
Fig. 17	Output of Computed Torque Control	36
Fig. 18	Position Error of Computed Torque Control	37
Fig. 19	Simulink Design of CTC w/ Disturbance	38
Fig. 20	Position Error of CTC w/ Disturbance	38
Fig. 21	Simulink Design of Disturbance Observer	41
Fig. 22	Simulink Design of CTC with Disturbance Observer	41
Fig. 23	Position Error of CTC with Disturbance Observer	42
Fig. 24	Position Error of CTC with Disturbance Observer @ $\tau=0.001$	43
Fig. 25	Position Error of CTC with Disturbance Observer @ $\tau=0.00001$	44
Fig. 26	Time Delay	45
Fig. 27	Notations	49
Fig. 28	Leg Physical Properties	50

INTRODUCTION

Modern control algorithms face not only stability criteria but also high speed operation requirements to ensure high productivity (throughput) in addition to precision and accuracy requirements for the reduced size components of mechanical devices. Robustness of control algorithm encompasses traditional controller parameters for variation of dynamic characteristics from one unit to another as well as many sophisticated control concepts that are capable of adapting to variation of characteristics during the operations.

Among many fundamental elements that significantly contribute to degradation of system performance, control engineers must confront the accuracy of the dynamic mathematical model on which the control algorithm is based. Accuracy of the model is becoming more stringent since the control design employs some of the modern design concepts mandating the model be highly accurate in order to achieve performance close to the theoretical estimation.

The discrepancy between the actual output and the output of the nominal model can be regarded as an equivalent disturbance applied to the nominal model. Professor Tomizuka of University of California Berkeley, Berkeley, California introduced the disturbance observer concept in his "Robotics and Automation" published in 1994, this concept was further researched by Professor Tesfaye of San Jose State University, San Jose, California in his 2000 research paper. The disturbance observer estimates the equivalent disturbance then the value of the estimate is utilized as a cancellation signal.

The disturbance observer concept presented by Professor Tomizuka will be analyzed and simulated using Matlab and Simulink before the concept is implemented on the high precision wafer stage with Computed Torque Controller. In the original paper published by Umeno and Hori (1991), the discussion was focused on the robustness and effectiveness of disturbance observer implemented on the system with two degrees of freedom; this paper will extend the concept to a system with six degrees of freedom.

Computed Torque Control determines the realistic acceleration torque according to the dynamic mathematical model of the manipulator and the desired motion, therefore, any modeling error in the dynamic mathematical model could significantly impact the motion response and stability of the total system.

A disturbance observer can improve the robustness of the control technique with the equivalent mass matrix fixed at a constant value during the operation. Numerous papers previously published support the concept that a disturbance observer can effectively suppress load variations with fixed nominal mass matrix, however, this concept has not been applied to a system with multiple degrees of freedom where the fixed mass matrix fails to decouple multiple axis disturbances applied to the system.

The proposed six degrees of freedom system is a Direct Write E-Beam Lithography System, a concept being researched and developed by Ion Diagnostics, Inc. located in Santa Clara, California. Direct Write E-Beam Lithography System is a next generation maskless lithography system for both drawing and inspecting integrated circuits utilizing direct-write electron beams capable of sub-100-nanometer resolutions.

The existing stage, a frictionless three legged structure must offer complete isolation from chamber vibrations and provide smooth and predictable motion holding all points on the surface of the wafer within one micrometer of the writing trajectory. Raster commanded trajectory describes a position in the three dimensional space as a function of time.

One of the main challenges is to obtain the nominal model for a system that possesses many known and unknown disturbances in a high voltage and high vacuum environment. High precision motion control design on a six DOF parametric dynamic mathematical model is to be simulated on a Simulink model with the equations of motion derived with both Newtonian and Lagrangian methods. Three dimensional orientation equations are obtained using Euler's equations of motion in three dimensions. Due to the complexity of the three legged design, a non-linear simulation model is designed with Simulink instead of analytical solutions using the equations of motion for the non-linear system.

This paper will introduce the basic theory on disturbance observer as presented by Professor Tomizuka, followed by a detailed description of the stage and derivation of the dynamic model. The subsequent section illustrates implementation of the disturbance observer concept on a six DOF mathematical model with simulation results. Computed Torque Control will be designed and the disturbance observer will be added to Computed Torque Controller to show the improvement in the performance of the system. The final section will summarize the effectiveness and performance of the disturbance observer.

Stage Design by Ion Diagnostics

Ion Diagnostics has designed a stage exclusively suited to the special requirements of the multi-column multi-beam (MxM) next generation electron beam lithography tool.

Special features of this stage include:

- Flexible joints
- Non-commutated linear motors
- Insulating ceramic legs
- Wings

The stage offers isolation from chamber vibration and provides smooth and predictable motion holding all points on the surface of the wafer within one micrometer of the writing trajectory.

The stage operates in high vacuum which is necessary for the electron beams to travel undisturbed while the wafer is subject to high voltage emitted by multiple electron beams during the writing process. The electron optic heads provide several micrometers of depth of focus and high-speed deflection feedback correction. The stage needs to follow its trajectory to within $\pm 1 \mu\text{m}$ for all points on the wafer. An advantage that this stage has over the conventional three axis stage is the small range of motion at virtually zero vibration.

There are five electromagnetic actuators providing six degrees of freedom of motion to the stage. The stage is positioned relative to the electron beam structure that is mounted to be an inertial reference. Instrumentation is attached to the writing structure,

namely three laser interferometers for X, Y, and yaw measurement (in the plane of the wafer), and three laser triangulation devices for Z (standoff), pitch, and roll measurement.

The flexible joints and non-commutated linear motors for motion in the wafer plane are possible because of the small range of motion required. The flexible joints are located at the top and bottom of three ceramic legs. The top joints connect to a wing structure holding the wafer chuck and the motor coils while the bottom joints connect to MinusK™ (commercially available vibration isolation spring) devices that provide vertical support and motion having a low spring rate. Voice coil motors in the support devices are the actuators for vertical, pitch, and roll control. Flexible joints, in contrast to rollers or sliding surfaces, provide extremely smooth and predictable motion.

Specification for 300mm wafer X-Y Stage:

- 50mm x 50mm travel, 100mm/s velocity
- +/-1 nm measurement accuracy (predicted position while following trajectory, at all points on the wafer)
- X acceleration at 0.5g, Y acceleration at 0.1g
- Yaw, Roll, Pitch displacement: +/- 0.005 radian
- Ultra High Vacuum environment, Wafer at high voltage: 75kV
- Interferometer velocity data to be used with data age position error of 30nm at 100mm/s
- Triangulation device to provide relative z position to control voice coils in z axis

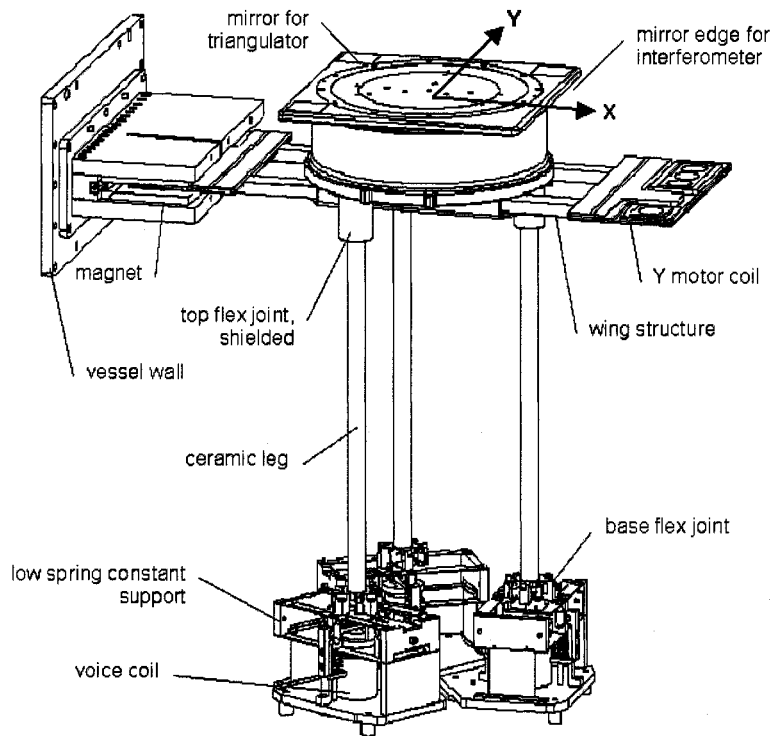


Fig. 1: Stage Schematic
Source: Ion Diagnostics

The basic structure of the stage is comprised of the following:

1. Ceramic Wafer Stage
2. Non-commutated Linear Drive provide x and y motion.
3. Three ceramic legs to support the stage
4. Three voice coils to provide z motion

The fundamental design concept of the three leg supported stage system is based on the following merits anticipated:

- The stage has no friction as it is practically levitated by three legs having the characteristics of inverted pendulum.

- A constant force spring is used to connect the leg to the voice coil that can completely eliminate the vibration originated from surrounding environment.
- The drive force exerted by the drive elements is directly transmitted to the stage.
- Within 50mm raster motion range, drive force distributions can be assumed uniform and linear.

Free Body Diagram:

Applied External Forces: X_1 & X_2 in x axis,
 Y_1 & Y_2 in y axis,
 Z_1 , Z_2 , and Z_3 in z axis.

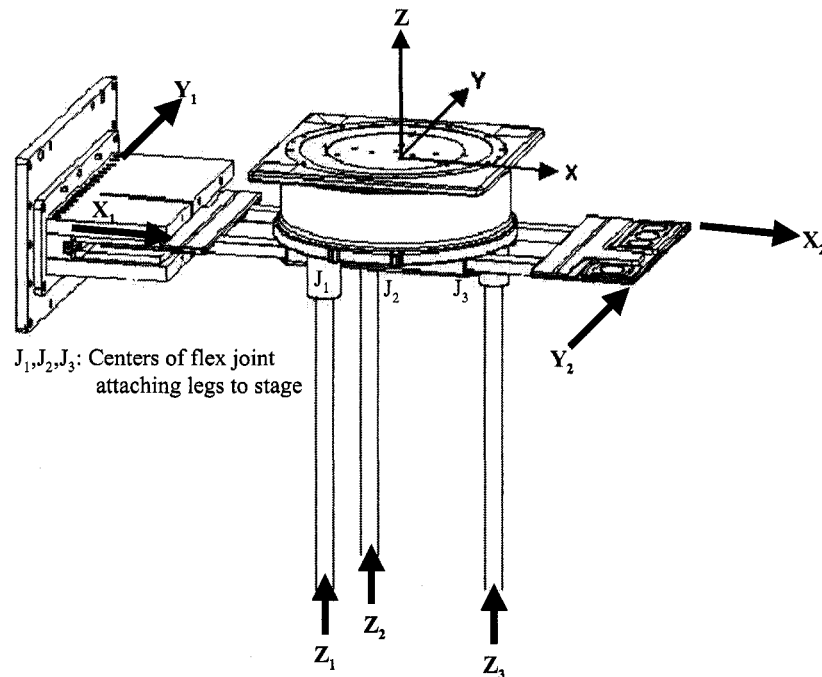
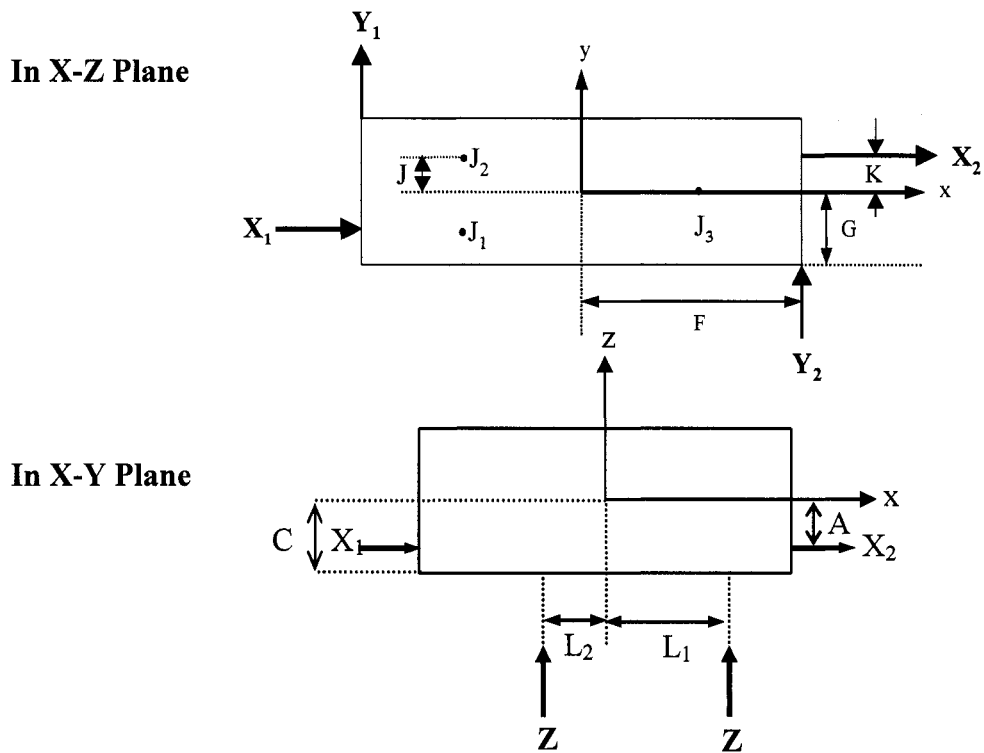


Fig. 2 Free Body Diagram of the Stage
 Source: Ion Diagnostics

There is one nitrogen cooled electromagnetic drive on each end providing forces in x $[x_1 x_2]$ and y $[y_1 y_2]$ direction while three voice coils attached to the end of each of the three legs provide forces in z $[z_1 z_2 z_3]$ direction. The theoretical drive force characteristics are determined by permeability theory, however, experimental data with respect to the applied current versus the thrust force characteristics including the thrust force distribution in the x-y plane will not be presented in this paper.

There are also gravitation forces acting on the system, from the weight of the stage and the weight of the legs. The reaction forces between the legs and the stage are applied at $J_1, J_2,$ and J_3 denoting connection points of three legs.

Dimension of the stage: (diagrams below not in scale)



In Y-Z Plane

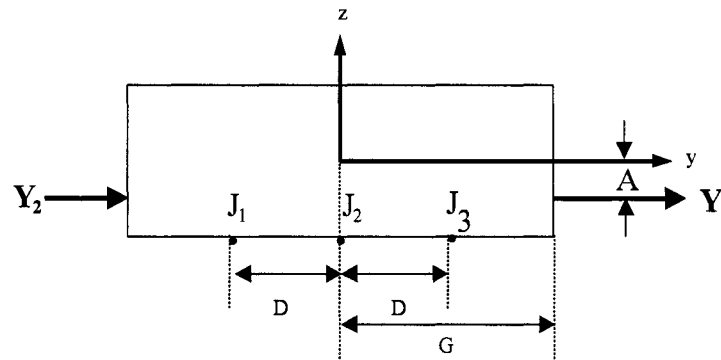


Fig. 3: Stage Dimensions

The development of the stage control systems was divided into two phases as described below:

Phase 1:

The initial control algorithm was to be developed without forces applied by the electron beams striking the substrate since the magnitude of the beam force was not determined until the final phase of the development. Also, there will be resistance forces caused by nitrogen cooling gas supply/return lines to the stage; the key factors include the bending radius, material of the line, and the gas pressure. Due to the lack of available information on the line, any forces caused by the cooling lines are to be disregarded in the phase 1.

Phase 2:

Both forces caused by the cooling lines and electron beams are time variant forces requiring a time variant control algorithm to be properly addressed. Neural Network or Repetitive teaching control is to be evaluated in the phase 2.

Dynamic Mathematical Model of the Stage

The wafer stage system is considered as a multi-rigid-body dynamic system, a set of dynamic equations describing the stage motion is derived. The equations of motion with respect to the body inertia frame is first derived in the form of Euler's equations of motion, then the coordinate transformation matrix is used to convert to the motion of the stage to the fixed inertia frame.

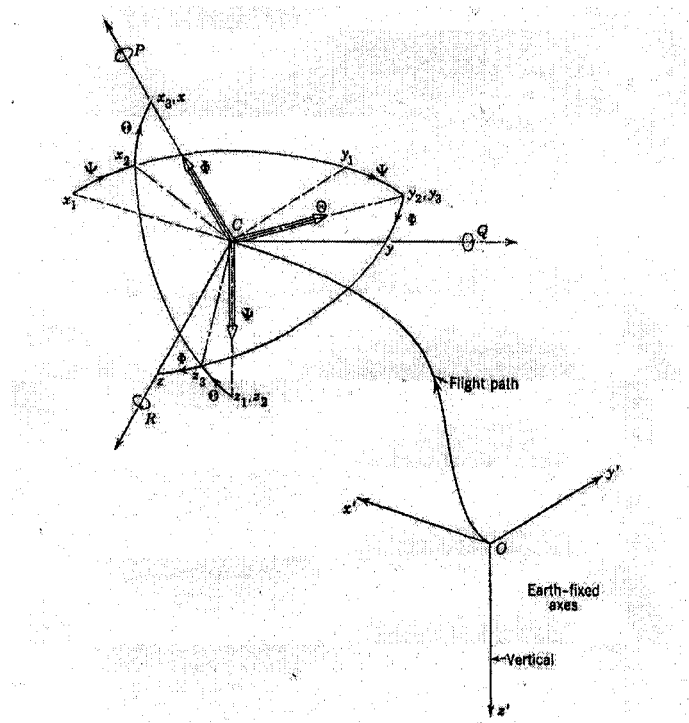


Fig. 4: Euler's EOM Coordinate Systems
Source: B. Etkin "Dynamic of Flight: Stability and Control"

Euler's equations of motion in three dimension can be found in many different forms, but the equations introduced in B. Etkin's "Dynamic of Flight: Stability and Control" was used to derive the equation of motion.

Notation:	L:	rolling moment
	M:	pitching moment
	N:	yawing moment
	P:	rolling velocity
	Q:	pitching velocity
	R:	yawing velocity
	X,Y,Z:	components of resulting force
	U,V,W:	components of velocity of the mass center

Fig. 4 defines the body axes centered at the mass center of the stage, the mass center is determined from the calculation carried out by Solid Works. Location of the center of mass and relevant dimensions are shown in Fig. 3.

Reaction Forces at the Joints

The forces acting on the joints connecting legs to the stage are expressed as $[F_x, F_y, F_z]_{i=1,2,3}$. Derivation of reaction forces at the joints are shown in Appendix 2. It must be noted that leg angles θ_{1x} and θ_{1y} are measured from the vertical inertia z axis to the position in the y-z and x-z plane. Variation of the angles between the legs is minor; however, derivation of the equations of motion treated each leg separately showing the angles for each leg explicitly.

Reaction forces at the joints are:

$$\begin{aligned} \text{Leg 1: } F_{x1} &= I_o(\ddot{x} - L_2\ddot{\theta}) + \frac{1}{H}(mg + Z_1)(x - L_2\theta) & \text{Eq 1} \\ F_{y1} &= I_o(\ddot{y} + D\ddot{\phi}) + \frac{1}{H}(mg + Z_1)(y + D\phi) \\ F_{z1} &= Z_1 - m(\ddot{z} + L_2\ddot{\theta} - D\ddot{\phi}) - mg + NLa_1 \end{aligned}$$

$$\text{Leg 2: } F_{x2} = I_o(\ddot{x} - L_2\ddot{\theta}) + \frac{1}{H}(mg + Z_2)(x - L_2\theta) \quad \text{Eq 2}$$

$$F_{y2} = I_o(\ddot{y} + D\ddot{\phi}) + \frac{1}{H}(mg + Z_2)(y + D\phi)$$

$$F_{z2} = Z_2 - m(\ddot{z} + L_2\ddot{\theta} + D\ddot{\phi}) - mg + NLa_2$$

$$\text{Leg 3: } F_{x3} = I_o(\ddot{x} - L_1\ddot{\theta}) + \frac{1}{H}(mg + Z_3)(x - L_1\theta) \quad \text{Eq 3}$$

$$F_{y3} = I_o(\ddot{y} + D\ddot{\phi}) + \frac{1}{H}(mg + Z_3)(y + D\phi)$$

$$F_{z3} = Z_3 - m(\ddot{z} - L_1\ddot{\theta}) - mg + NLa_3$$

Please refer to Appendix 1 for values for variables above.

NLa_1 , NLa_2 , and NLa_3 are non-linear terms in the form of $NLa = -\left(\frac{2I_{yy}}{H} + \frac{H}{2}m\right)\ddot{\theta}_{1y}\theta_{1y}$

Non linear product of angular acceleration and angular displacement terms will be considered as a disturbance to the nominal plant. The magnitudes of these terms are negligible compared to the forces acting on the stage; elimination of these terms does not affect the performance of the mathematical model during the simulation.

External Forces and Moments Acting on the Stage

The stage is subject to six degrees of freedom; Euler's angle uses X,Y,Z for translation motion with L, M, N for rotation motion. L, M, N is equivalent to roll, pitch, and yaw respectively.

The term external forces and moments are due to the fact that forces acting on z-axis are transmitted through three legs to flexible joints which affect the motion of the stage in all six axes.

Equations for the external forces and moments

$$\begin{aligned}
 X &= -(F_{x1} + F_{x2} + F_{x3}) + X_1 + X_2 & \text{Eq 4} \\
 Y &= -(F_{y1} + F_{y2} + F_{y3}) + Y_1 + Y_2 \\
 Z &= F_{z1} + F_{z2} + F_{z3} \\
 L &= (Y_1 + Y_2)A + (F_{z2} - F_{z1})D - (F_{y1} + F_{y2} + F_{y3})C \\
 M &= (F_{x1} + F_{x2} + F_{x3})C - F_{z3}L_1 + (F_{z1} + F_{z2})L_2 - (X_1 + X_2)A \\
 N &= (F_{x2} - F_{x1})J - F_{y3}L_1 + (F_{y1} + F_{y2})L_2 - (x_1 - x_2)K + (Y_2 - Y_1)F
 \end{aligned}$$

These equations are applied to Euler's equation of motion presented by B. Etkin.

$$\begin{aligned}
 X + M_s g \sin \theta &= M_s (\dot{U} + QW - RV) & \text{Eq 5} \\
 Y - M_s g \cos \theta \cos \theta &= M_s (\dot{V} + RU - PW) \\
 Z - (M_s + 3m) g \cos \theta \cos \theta &= M_s (\dot{W} + PV - QU)
 \end{aligned}$$

$$\begin{aligned}
 L &= I_{s_{xx}} \dot{P} - I_{s_{xz}} \dot{R} + (I_{s_{zz}} - I_{s_{yy}})QR - I_{s_{xz}} PQ \\
 M &= I_{s_{yy}} \dot{Q} + (I_{s_{xx}} - I_{s_{zz}})RP + I_{s_{xz}} (P^2 - R^2) \\
 N &= -I_{s_{xz}} \dot{P} + I_{s_{zz}} \dot{R} + (I_{s_{yy}} - I_{s_{xx}})PQ + I_{s_{xz}} QR
 \end{aligned}$$

where

$$\begin{aligned}
 P &= \dot{\phi} - \dot{\psi} \sin \theta \\
 Q &= \dot{\theta} \cos \phi + \dot{\psi} \cos \theta \sin \theta \\
 R &= \dot{\psi} \cos \theta \sin \theta - \dot{\theta} \sin \phi
 \end{aligned}$$

$$\begin{aligned}
\dot{\theta} &= Q\cos\varphi - R\sin\varphi \\
\dot{\phi} &= P + Q\sin\varphi\sin\theta + R\cos\varphi\cos\theta \\
\dot{\psi} &= (Q\sin\varphi + R\cos\varphi)\sec\theta
\end{aligned}$$

Please refer to Appendix 2 for a detailed presentation of the equations of motion.

In expressing external forces and moments in terms of Euler's angles, the following expressions can be obtained for each axis.

Forces acting on x-axis:

$$\begin{aligned}
X_1 + X_2 &= (3I_o + M_s)\ddot{x} - 3I_oL_1\ddot{\theta} + \frac{3mg}{H}x + \frac{9mgL_1}{H}\theta - M_s g\sin\theta \\
&+ \frac{1}{H}(Z_1 + Z_2 + Z_3)x - \frac{1}{H}(L_2Z_1 + L_2Z_2 + L_1Z_3)\theta + M_s(\dot{\theta}\dot{z} - \dot{\psi}\dot{y})
\end{aligned} \quad \text{Eq 6}$$

Forces acting on y-axis:

$$\begin{aligned}
Y_1 + Y_2 &= (3I_o + M_s)\ddot{y} + 3I_oD\ddot{\phi} + \frac{3mg}{H}y + \frac{3mgD}{H}\phi + \frac{1}{H}(Z_1 + Z_2 + Z_3)y \\
&+ \frac{1}{H}(Z_1 + Z_2 + Z_3)D\phi + M_s g\cos\theta\cos\theta + M_s(\dot{\psi}\dot{x} - \dot{\phi}\dot{z})
\end{aligned} \quad \text{Eq 7}$$

Forces acting on z-axis:

$$\begin{aligned}
Z_1 + Z_2 + Z_3 &= (M_s + 3m)\ddot{z} + 5mL_1\ddot{\theta} + 3mg + (M_s + 3m)g\cos\theta\cos\theta \\
&+ M_s(\dot{\phi}\dot{y} - \dot{\theta}\dot{z}) - NLa_T
\end{aligned} \quad \text{Eq 8}$$

$$\text{where } NLa_T = NLa_1 + NLa_2 + NLa_3$$

Moments around y-axis:

$$\begin{aligned}
(Y_1 + Y_2)A &= 3I_oC\ddot{y} + (3I_oCD + 2D^2m + Is_{xx})\ddot{\phi} - Is_{xz}\ddot{\psi} + \frac{3mgC}{H}y + \frac{3mgCD}{H}\phi \\
&+ \frac{C}{H}(Z_1 + Z_2 + Z_3)y + \frac{DC}{H}(Z_1 + Z_2 + Z_3)\phi + (Is_{zz} - Is_{yy})\dot{\theta}\dot{\psi} - Is_{xz}\dot{\phi}\dot{\theta} - (NLa_2 - NLa_1)D
\end{aligned} \quad \text{Eq 9}$$

Moments around x-axis:

$$\begin{aligned}
 (Z_1 + Z_2)L_2 - L_1Z_3 = & -3I_oC\ddot{x} + 5mL_1\ddot{z} + [3I_oL_1C - 3mL_1^2 + I_{s_{yy}}]\ddot{\theta} & \text{Eq 10} \\
 & - \frac{3mgC}{H}x - \frac{9mgCL_1}{H}\theta + 3L_1mg + (I_{s_{xx}} - I_{s_{zz}})\dot{\psi}\dot{\phi} + I_{s_{xz}}(\dot{\phi}^2 - \dot{\psi}^2) \\
 & - \frac{C}{H}(Z_1 + Z_2 + Z_3)x + \frac{C}{H}(L_2Z_1 + L_2Z_2 + L_1Z_3)\theta - L_1NL_{a_3} + L_2(NL_{a_1} + NL_{a_2})
 \end{aligned}$$

Moments around z-axis:

$$\begin{aligned}
 (X_2 - X_1)K + (Y_2 - Y_1)F = & -3I_oL_1\ddot{y} - [3I_oDL_1 + I_{xz}]\ddot{\phi} + I_{zz}\ddot{\psi} & \text{Eq 11} \\
 & - \frac{3L_1}{H}mgy - \frac{3L_1}{H}mgD\phi - \frac{3Z_3L_1}{H}(y + D\phi) + I_{xz}\dot{\theta}\dot{\psi} + (I_{s_{yy}} - I_{s_{xx}})\dot{\phi}\dot{\theta}
 \end{aligned}$$

Vector Equations of Motion

The above equations can be put into the form:

$$M\ddot{q} + N(q, \dot{q}) + G(q) = WF = \tau \quad \text{Eq 12}$$

M is a mass matrix, N a non linear matrix, G a gravity matrix, τ is an external force matrix represented by force distribution matrix W multiplied by actuator force vector of F.

Non linear term N can be represented by

$$N(q, \dot{q}) = N_1q + N_2(\dot{q}) \quad \text{Eq 13}$$

here $q = [x, y, z, \phi, \theta, \psi]^T$

Mass matrix M

$$\begin{pmatrix} 3I_0+Ms & 0 & 0 & 0 & -3I_0L_1 & 0 \\ 0 & 3I_0+Ms & 0 & 3I_0D & 0 & 0 \\ 0 & 0 & Ms+3m & 0 & 3mL_1 & 0 \\ 0 & 3I_0C & 0 & 3 I_0CD+2D^2 L_1+I_{xx} & 0 & -I_{xz} \\ 0 & 0 & 5mL_1 & 0 & 3 I_0C L_1-3mL_1^2+I_{yy} & 0 \\ 0 & -3I_0L_1 & 0 & 3 I_0DL_1+I_{xz} & 0 & I_{zz} \end{pmatrix}$$

Non Linear Matrix N₁

$$\begin{pmatrix} (3mg+Z_1+Z_2+Z_3)/H & 0 & 0 & 0 & -[9mg L_1+ L_2(Z_1+Z_2)+ L_1Z_3]/H & 0 \\ 0 & (3mg+Z_1+Z_2+Z_3)/H & 0 & D(3mg+Z_1+Z_2+Z_3)/H & 0 & 0 \\ 0 & 0 & 0 & 0 & 0 & 0 \\ 0 & C(3mg+Z_1+Z_2+Z_3)/H & 0 & C(3mg+Z_1+Z_2+Z_3)/H & 0 & 0 \\ C(3mg-Z_1-Z_2-Z_3)/H & 0 & 0 & 0 & -C[9mg L_1+ L_2(Z_1+Z_2)+ L_1Z_3]/H & 0 \\ 0 & 3L_1(mg-Z_3)/H & 0 & -3DL_1(mg-Z_3)/H & 0 & 0 \end{pmatrix}$$

$N_2(\dot{q})$ Matrix

$$\begin{pmatrix} Ms(\dot{\theta} z - \dot{\phi} y) \\ Ms(\dot{\phi} x - \dot{\theta} z) \\ Ms(\dot{\phi} y - \dot{\theta} z) \\ (I_z - I_{yy})\dot{\theta} \dot{\phi} - I_{xz}\dot{\phi} \dot{\theta} \\ (I_{xx} - I_{zz})\dot{\phi} \dot{\phi} - I_{xz}(\dot{\phi}^2 - \dot{\theta}^2) \\ I_{xz}\dot{\theta} \dot{\phi} \end{pmatrix}$$

$G(q)$ matrix

$$\begin{pmatrix} -Msg \sin\theta \\ Msg \cos\theta \sin\phi \\ (Ms+3m)g \cos\theta \cos\phi \\ 0 \\ 3mgL_1 \\ 0 \end{pmatrix}$$

W Matrix and F vector

$$W = \begin{pmatrix} 1 & 1 & 0 & 0 & 0 & 0 & 0 \\ 0 & 0 & 1 & 1 & 0 & 0 & 0 \\ 0 & 0 & 0 & 0 & 1 & 1 & 1 \\ 0 & 0 & A & A & 0 & 0 & 0 \\ 0 & 0 & 0 & 0 & L_2 & L_2 & -L_1 \\ -K & K & -F & F & 0 & 0 & 0 \end{pmatrix} \quad F = \begin{pmatrix} X_1 \\ X_2 \\ Y_1 \\ Y_2 \\ Z_1 \\ Z_2 \\ Z_3 \end{pmatrix}$$

Above figure, $[\ddot{q}_d, \dot{q}_d, q_d]$ represent the desired trajectory in the three dimensional space for the stage to follow. The equation of motion to describe the dynamic of the system is:

$$M\ddot{q} + N(q, \dot{q}) + G(q) + \tau_d = \tau(t) = WF(t),$$

where τ_d includes both the modeling error and the process noise.

Computed Torque Control signal τ can be derived as:

$$\tau = M\ddot{q} + N(q, \dot{q}) + G(q) + Mu(t)$$

where the feedback control signal $u(t)$ generated by the servo control loop can be expressed in terms of proportional gain and derivative gain:

$$u(t) = -K_p E(t) - K_v \dot{E}(t) \quad (\text{note that the integral term } -K_i \int E(t)dt \text{ can be added})$$

where $E(t) = q_d(t) - q(t)$, $q(t) = [x, y, z, \phi, \theta, \varphi]^T$

The objective of the motion control system is to have the stage follow the desired trajectory of $x(t)$ and $y(t)$ within the acceptable tolerance while $[z, \phi, \theta, \varphi]^T$ motions are constrained to zero. By substituting the above equation, it can be readily seen that:

$$\ddot{E}(t) = u(t) - \tau_d(t)$$

τ_d in the above equation prevents the decoupling of the dynamic equation, this presents a great deal of difficulty in designing a control system.

However, if τ_d is ignored, then the state dynamic equations can be decoupled allowing all control loops to be individually designed. By designing a control system which can compensate for inaccuracies in dynamic modeling of the plant, τ_d can be ignored during

Computed Torque Control design step. Any inaccuracies in the dynamic modeling are to be compensated by disturbance observers in each loop.

The state dynamic form of the above equation is:

$$\dot{x} = \begin{bmatrix} 0 & I \\ 0 & 0 \end{bmatrix} x + \begin{bmatrix} 0 \\ I \end{bmatrix} u + \begin{bmatrix} 0 \\ -I \end{bmatrix} \tau_d \quad \text{Eq 14}$$

Where $X=(E, \dot{E})^T$

Plant matrix is controllable which allows the pole placement method to be used to obtain the best set of the feedback gain $[K_p K_v]$, then the servo control loop will be in the form of:

$$u(t) = -K_p E - K_v \dot{E} \quad \text{which yields}$$

$$\ddot{E} + K_v \dot{E} + K_p E = 0 \rightarrow \text{here } \tau_d \text{ is ignored.}$$

It is important to note that since τ_d is ignored, the robustness of the servo loop is not optimized, nor the performance of Computed Torque Controller. A disturbance observer with robust control approach will predict the ignored term τ_d in addition to inaccuracies in the dynamic mathematical model.

Disturbance Observer Theory

The accuracy of a mathematical model generated either to derive the control algorithm or to simulate the system plays an important role in validating the system performance. The disturbance observer is designed to estimate the difference between the actual output and the nominal model output, and to use this information to generate a cancellation signal to minimize the dynamic effect of the difference.

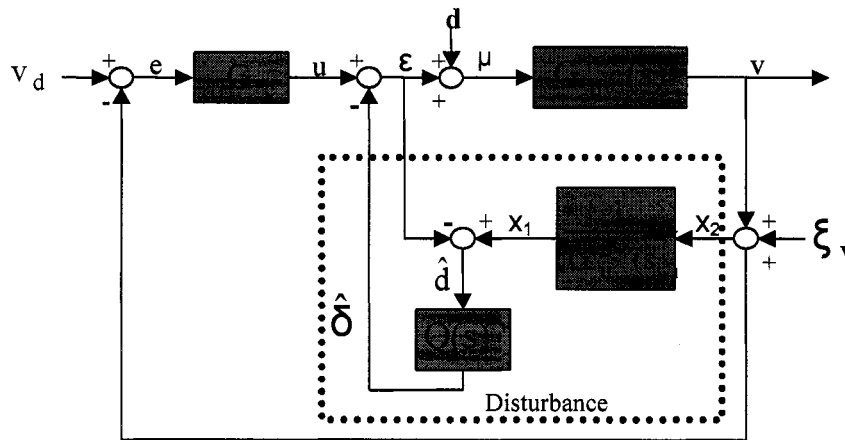


Fig. 6: Block Diagram of Disturbance observer

Mathematical Derivation of Disturbance Observer

G_{uv} : Actual Transfer Function

G_{uv}^n : Nominal Transfer Function

d : Nonlinear disturbance not compensated

ξ_v : Measurement Noise

v : Velocity Output

From the figure above, when $Q(s)=1$, the transfer function of the system will be

$$\hat{\delta} = \hat{d} = \left[1 - \frac{G_{uv}^n}{G_{uv}}\right]u + \frac{1}{G_{uv}^n} \xi_v + d \quad \text{Eq 15}$$

The derivation of the above equation is as follows:

The velocity output can be expressed as

$$\begin{aligned} v &= G_{uv} \mu & \mu &= d + \varepsilon & \text{Eq 16} \\ &= G_{uv}(d + \varepsilon) & \varepsilon &= u - \hat{\delta} \\ &= G_{uv}(d + u - \hat{\delta}) \end{aligned}$$

$$\text{Let } x_1 = v + \xi_v$$

$$\text{And } x_2 = \frac{1}{G_{uv}^n(s)} x_1 = \frac{1}{G_{uv}^n} (v + \xi_v) = \frac{1}{G_{uv}^n} \{[G_{uv}(d + u - \hat{\delta})] + \xi_v\} \quad \text{Eq 17}$$

$$\hat{d} = x_2 - \varepsilon = \frac{1}{G_{uv}^n} \{[G_{uv}(d + u - \hat{\delta})] + \xi_v\} - \varepsilon$$

$$\hat{\delta} = \hat{d} \text{ where } Q(s)=1$$

$$\hat{\delta} = \frac{G_{uv}}{G_{uv}^n} d + \frac{G_{uv}}{G_{uv}^n} u - \frac{G_{uv}}{G_{uv}^n} \hat{\delta} + \frac{\xi}{G_{uv}^n} - (u - \hat{\delta}) \quad \text{Eq 18}$$

$$\frac{G_{uv}}{G_{uv}^n} \hat{\delta} = \left(\frac{G_{uv}}{G_{uv}^n} - 1\right)u + \frac{1}{G_{uv}^n} \xi_v + \frac{G_{uv}}{G_{uv}^n} d$$

$$\begin{aligned} \hat{\delta} &= \frac{G_{uv}^n}{G_{uv}} \left(\frac{G_{uv}}{G_{uv}^n} - 1\right)u + \frac{1}{G_{uv}} \xi_v + d \\ &= \left(1 - \frac{G_{uv}^n}{G_{uv}}\right)u + \frac{1}{G_{uv}} \xi_v + d \end{aligned}$$

Next the velocity output is then expressed as

$$\begin{aligned} v &= G_{uv}\mu = G_{uv}(\varepsilon + d) = G_{uv}(d + u - \hat{d}) \quad Q = 1 \text{ and } \hat{d} = \delta \\ &= G_{uv}(u - \hat{d} + d) \end{aligned} \quad \text{Eq 19}$$

now,

$$\begin{aligned} x_1 &= v + \xi_v \\ v &= x_1 - \xi_v \quad \text{where} \quad x_2 = \frac{1}{G_{uv}^n} x_1 \quad x_1 = G_{uv}^n x_2 \\ &= G_{uv}^n x_2 - \xi_v \quad \hat{d} = x_2 - \varepsilon = x_2 - u + \delta = x_2 - u + \hat{d} \\ &= G_{uv}^n u - \xi_v \quad x_2 = u \end{aligned}$$

$$\therefore v = \mathbf{G}_{uv}(\mathbf{u} - \hat{\mathbf{d}} + \mathbf{d}) = \mathbf{G}_{uv}^n \mathbf{u} - \xi_v \quad \text{Eq 20}$$

Eq 20 shows that the input-output relation between u and v as characterized by the nominal model.

From the figure 6, the following relation can be established

$$v = G_{uv}^0(s)u + G_{uv}^0(s)d + G_{\xi_v}^0(s)\xi_v \quad \text{Eq 21}$$

where

$$G_{uv}^0 = \frac{G_{uv}G_{uv}^n}{G_{uv}^n + (G_{uv} - G_{uv}^n)Q}, \quad G_{dv}^0 = \frac{G_{uv}G_{uv}^n(1-Q)}{G_{uv}^n + (G_{uv} - G_{uv}^n)Q},$$

and $G_{\xi_v}^0 = \frac{G_{uv}Q}{G_{uv}^n + (G_{uv} - G_{uv}^n)Q}$

if $Q(s) \approx 1$, the three transfer functions above are

$$G_{uv}^0 = G_{uv}^n, \quad G_{dv}^0 = 0, \quad G_{\xi_v}^0 = -1 \quad \text{Eq 22}$$

and the relation in Eq 20 is resumed. On the other hand, if $Q(s)=0$, the three transfer functions are

$$G_{uv}^0 = G_{uv}, \quad G_{dv}^0 = G_{uv}, \quad G_{\xi_{vV}}^0 = 0$$

and the open loop dynamics is resumed. Professor Tomizuka recommended allowing the low frequency dynamics of $Q(s)$ to be close to 1 for disturbance rejection and the model inaccuracy compensation. For the high frequency dynamics, $Q(s)$ needs to be close to 0 in order to bring the relative order of $Q(s)$ equal or greater than that of $G_{uv}^n(s)$.

Umeno & Hori stated that $(1-Q(s))$ and $Q(s)$ can be interpreted as a sensitivity function and complementary sensitivity function for the velocity feedback loop, and suggested $Q(s)$ in the form of:

$$Q(s) = \frac{1 + \sum_{k=1}^{N-r} a_k (\tau s)^k}{1 + \sum_{k=1}^N a_k (\tau s)^k} \quad \text{here, } \tau \text{ determines the cutoff frequency of the } Q \text{ filter.}$$

Umeno & Hori further suggested employing a Butterworth filter design in where $Q(s)$ is defined such that $1-Q(s)$ has the frequency characteristics of a high pass filter.

Figure 7 shows Bode plot $Q(s)$ by the order.

Parameter $Q(s)$

Type 0:
$$Q(s) = \frac{1}{s\tau + 1}$$

Type 1:
$$Q(s) = \frac{1.41(s\tau) + 1}{(s\tau)^2 + 1.41(s\tau) + 1}$$

Type 2:
$$Q(s) = \frac{2(s\tau)^2 + 2(s\tau) + 1}{(s\tau)^3 + 2(s\tau)^2 + 2(s\tau) + 1}$$

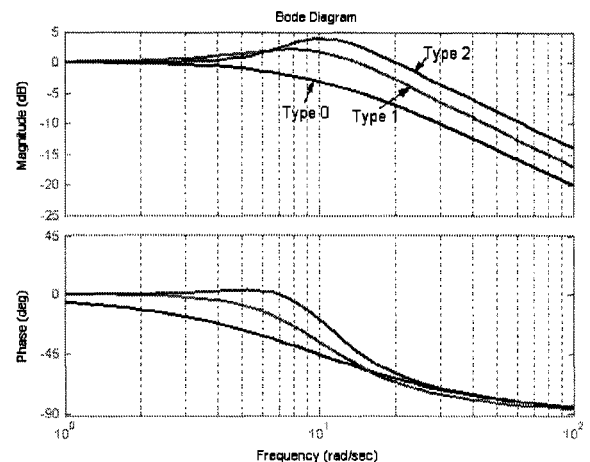


Fig. 7: Bode Plot of Q filters

From the Bode Plot above, it is clear that by selecting proper cutoff frequency τ , both magnitudes and phase angles can be shifted.

The conventional PI controller is equivalent to type 0 since it can be derived by setting $Q(s)=0$. Close comparison of three types of Q filters reveals that it is difficult to recognize the superiority of any one type of filter over another. The cutoff frequency determines the sensitivity of the observer. The observer's basic design employs a Butterworth filter design.

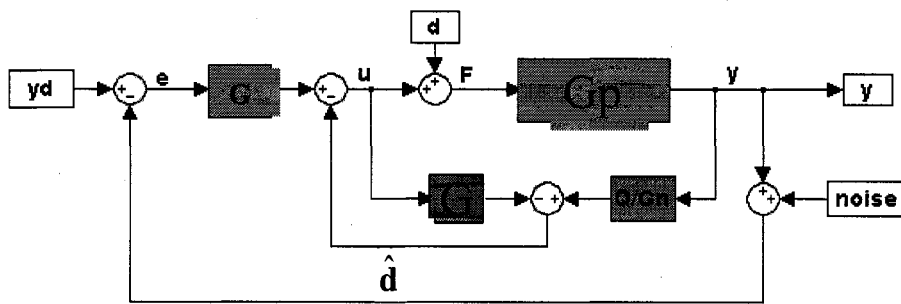


Fig 8: Block Diagram of Disturbance Observer w/ Filter

Robustness of $Q(s)$ parameter was simulated using Simulink, as the disturbance d was applied to the plant G_p , the disturbance observer measures the difference between output y and control signal u which is utilized as a cancellation signal.

The following relations can be readily seen.

$$G_{uy} = \frac{y}{u} = \frac{G_p G_n}{\Delta}$$

$$G_{dy} = \frac{y}{d} = \frac{G_p G_n (1-Q)}{\Delta} \quad \text{Eq 23}$$

$$G_{ny} = \frac{y}{N} = \frac{G_p Q}{\Delta}$$

$$\Delta = G_n + Q(G_p - G_n)$$

low frequency : $Q \rightarrow 1 \quad G_{uy} = G_n, G_{dy} = 0$

high frequency : $Q \rightarrow 0 \quad G_{ny} = 0$

As an example, the figure below illustrates Simulink diagram that was used to generate simulation data. Both references and disturbances are step functions.

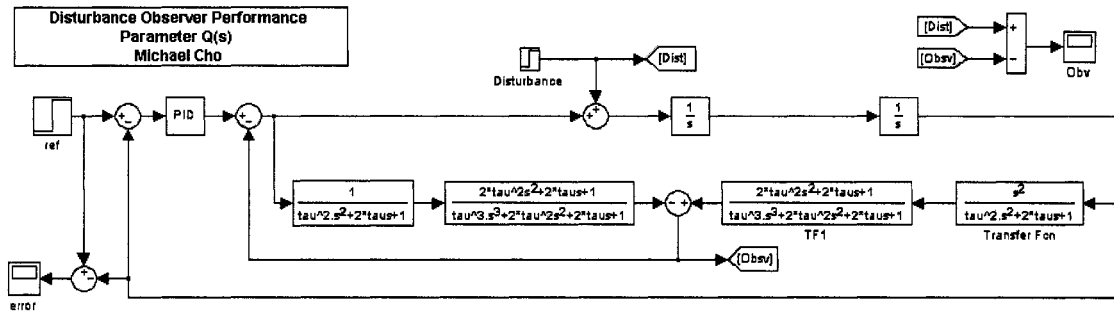


Fig. 9: Simulation Diagram with Double Integrator

$\frac{1}{\tau^2 s^2 + 2\tau s + 1}$ is added to make the system realizable.

The disturbance observer cannot be implemented if $Q(s)=1$ since $\frac{1}{G_{uv}^n}$ is not realizable by itself. Instead $Q(s)/G_{uv}^n(s)$ can be made realizable by making the relative order of $Q(s)$ equal or greater than the order of $G_{uv}^n(s)$.

As an example, a plant of a simple double integrator is designed with a PD controller. Figure 10 shows the performance of the parameter $Q(s)$. Step input of 50 was given with step disturbance of 50, the results are shown below.

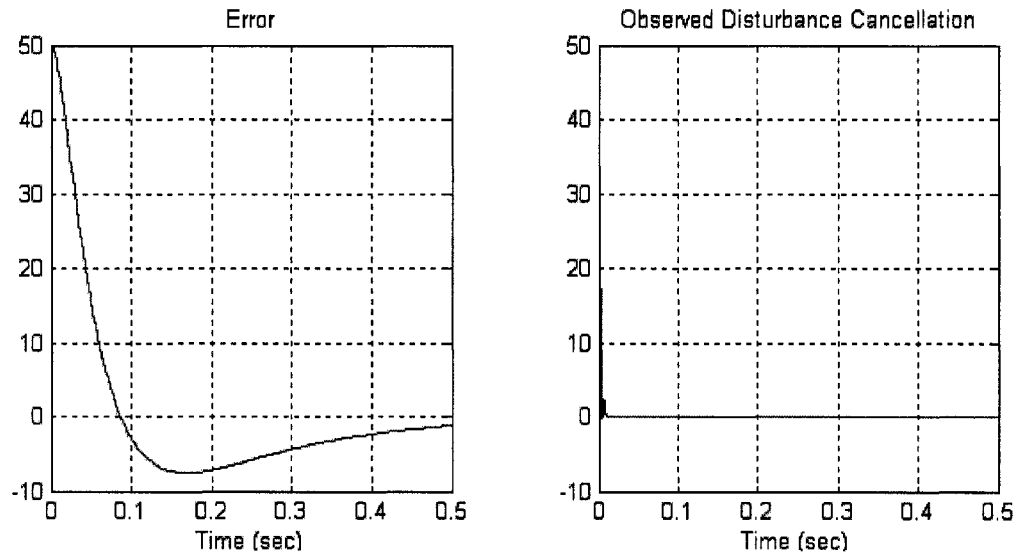


Fig. 10: Simulation Output of Double Integrator

Error is the difference between the desired outputs versus the actual output while the observed disturbance cancellation signal displays the output of the disturbance observer. It can be seen that the disturbance observer effectively estimates the magnitude of the disturbance signal, then utilizes the signal to generate a cancellation signal.

The disturbance observer cancels the disturbance signal in 0.01 second while error signal is still driving toward full cancellation after 0.5 second; this slow response is due to the performance of the PD controller not being properly tuned.

State Space Dynamic Equations

Vector equations of motion $M\ddot{q} + N_1\dot{q} + N_2(q) + G(q) = WF = \tau$ can be converted to state space dynamic equations in the form of $\dot{X} = AX + BU + f$ where $X = [q \ \dot{q}]^T$, $U = F$.

$$\dot{X} = \begin{bmatrix} 0 & I \\ -M^{-1}N_1 & 0 \end{bmatrix} X + \begin{bmatrix} 0 \\ -M^{-1}W \end{bmatrix} U + \begin{bmatrix} 0 \\ -M^{-1} \end{bmatrix} G(q) + \begin{bmatrix} 0 \\ -M^{-1} \end{bmatrix} N^2(\dot{q}) \quad \text{Eq 24}$$

The measurement equation is $Y = CX + DU$, C is assumed to be an identity matrix, and D to be a zero matrix for the purpose of simulation.

Matrix A is the system matrix, where $A = \begin{bmatrix} 0 & I \\ -M^{-1}N_1 & 0 \end{bmatrix}$ which explicitly indicates that the stability of the systems is affected by non linear terms N_1 . The term N_1 contains forces from z actuators to counterbalance the forces from gravity in addition to apply forces to maintain the top surface of the stage normal to the z axis. Forces from three voice coils supporting the three legs will have impact on the stability of the stage.

Suppose no forces from z actuators, then the N_1 matrix will be in the form of,

$$\begin{pmatrix} 3mg/H & 0 & 0 & 0 & -9mgL_1/H & \\ 0 & 3mg/H & 0 & 3mgD/H & 0 & 0 \\ 0 & 0 & 0 & 0 & 0 & 0 \\ 0 & 3mgC/H & 0 & 3mgC/H & 0 & 0 \\ 3mgC/H & 0 & 0 & 0 & -9mgCL_1/H & 0 \\ 0 & 0 & 3mgL_1/H & 3mgDL_1/H & 0 & 0 \end{pmatrix}$$

The stability of matrix A can be tested using many different methods; this can be also measured by building a plant in Simulink. Simulink can simulate a dynamic system as long as there is sufficient force in the z-direction to counterbalance the gravity force.

Trajectory Generation

The desired trajectory of the stage is raster trajectory, 50mm travel in x axis, then 50mm travel in y axis as shown in Fig. 11.

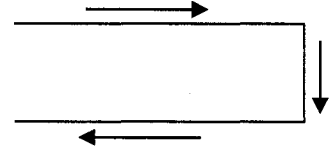


Fig. 11: Raster Trajectory

The maximum velocity of the stage is 100mm/s with 0.5g (4.9m/s²) acceleration in x axis and 0.1g (0.98m/s²) acceleration in y axis. A linear Function with Parabolic Blends (LFPB) was used to generate the desired trajectory, then the first derivate of the position with respect to time became the desired velocity trajectory, and the second derivative of position with respect to time became the desired acceleration trajectory.

The desired position can be obtained:

$$q_{d_i}(t) = \begin{cases} a_i + (t - t_k)b_i + (t - t_k)^2 c_i, & \text{full acceleration} \\ d_i + v_i t, & \text{constant velocity} \\ e_i + (t - t_{k+1})f_i + (t - t_{k+1})^2 g_i & \text{full deceleration} \end{cases}$$

The coefficient v_i may be interpreted as the maximum velocity allowed, the design parameters are v_i and the duration of the acceleration t_b . The remaining coefficients can be obtained:

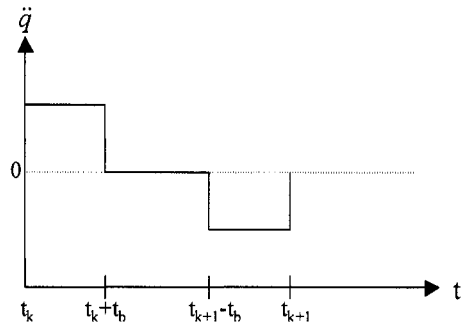


Fig. 12: Trajectory of Acceleration by LFPB

$$\begin{aligned}
a_i &= q_i(t_k), & b_i &= \dot{q}_i(t_k), & c_i &= \frac{v_i - \dot{q}_i(t_k)}{2t_b} \\
d_i &= \frac{q_i(t_k) + q_i(t_{k+1}) - v_i t_{k+1}}{2} \\
e_i &= q_i(t_{k+1}), & f_i &= \dot{q}_i(t_{k+1}) \\
g_i &= \frac{v_i t_{k+1} + q_i(t_k) - q_i(t_{k+1}) - v_i t_{k+1} + 2t_b[(\dot{q}_i(t_{k+1}) - v_i)]}{2t_b^2}
\end{aligned}$$

The above equation will yield the trajectory of the desired position. By using Matlab, the matrix of the position against the time was generated, and then this matrix was differentiated once for the velocity matrix and twice the acceleration matrix from Simulink. These matrices were plotted below in Fig. 13.

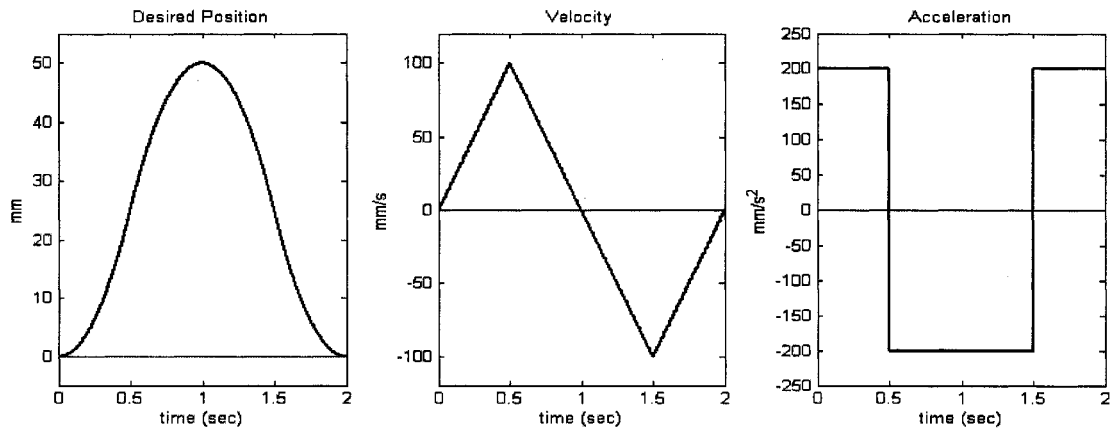


Fig. 13: Trajectory of LFPB

The trajectory generated by LFPB presented implementation problems in real time operation including torque generation that is not realizable. As it can be seen from the plot above, torque generation is similar to square wave format implying torque must be reversed from 200mm/s^2 to negative 200mm/s^2 instantaneously, this is a challenging issue with actuators.

In order to alleviate any potential problems with the actuators due to the unrealizable torque curve, a more realistic torque curve was generated by simply creating a matrix that contains a sine curve shaped torque profile. Acceleration and deceleration curves are in a sine curve form with a maximum acceleration of 4m/s^2 . Once the torque matrix is created, values were integrated to generate a velocity profile with maximum velocity of 100mm/s .

The raster motion requires 50mm travel in x direction given maximum acceleration of $0.5g$ and maximum velocity of 100mm/s . The sine curved torque profile integrated twice yields position profile in x-direction with elapsed time of approximately 1.5 sec for a complete raster loop. Plots of trajectory shown below in Fig. 14.

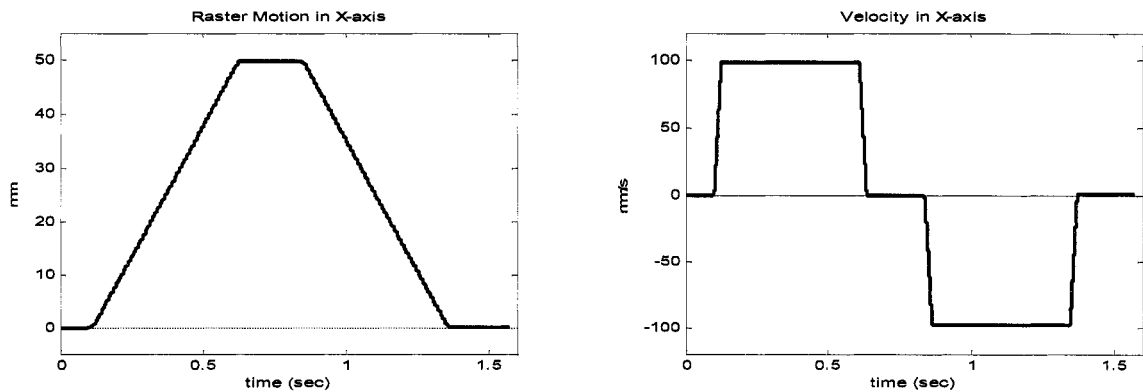


Fig. 14: Sinusoidal Position and Velocity Profile

And the torque profile:

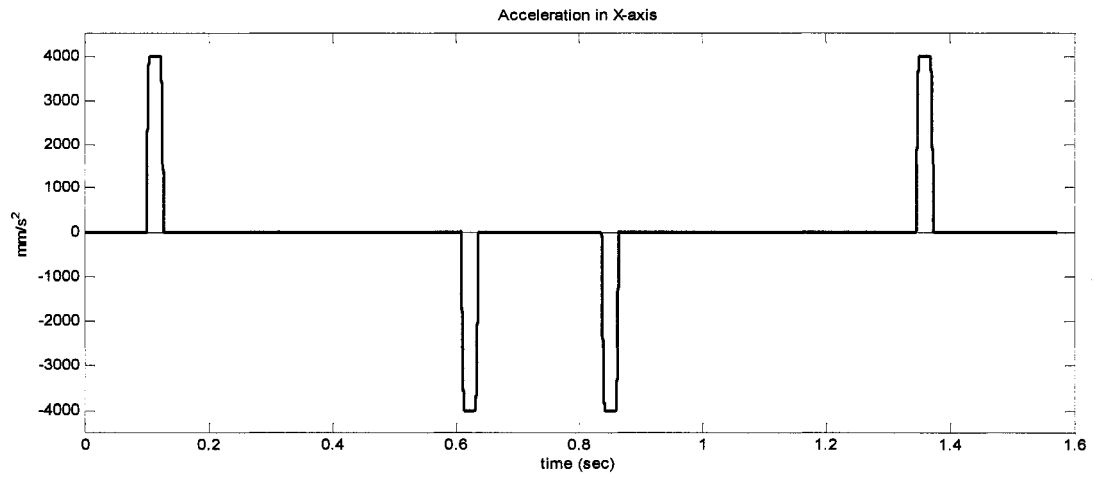


Fig. 15: Sinusoidal Torque Profile

Position, velocity, and torque matrices generated above are to be used as desired reference points for Computed Torque Control scheme.

Simulation Analysis of Computed Torque Controller

Based on the dynamic mathematical model presented in the previous section, a Simulink model is built to simulate the performance of a system with Computed Torque Controller. Simulations have the following conditions applied:

Trajectory: Motion only in the x-axis while maintaining the y-axis constant. Also the controller must maintain the wafer surface perfectly normal to the z axis. For the first simulation, matrices in x-axis contain non-zero terms as shown in the "Trajectory Generation" section, however, for other axes, all the desired reference input matrices contain all zero elements. This trajectory is consistent with the raster motion specified which allows motion in one axis at a time.

The control system is designed to have the closed loop system behave as a critically damped system by selecting $K=[K_p, K_v]$. This pole placement method can be used only when the plant is controllable.

Matlab command "place" is used with the following desired pole.

```
P=-3000*[3 2.99 2.98 2.97 2.96 2.95 4.10 4.09 4.08 4.07 4.06 4.05];
```

Then, the following Ks are generated:

```
Kp = 1.0e+008 *
```

```
1.0860  0.0029 -0.0003  0.0019  0.0002  0.0005
0.0028  1.0938  0.0029 -0.0007 -0.0004 -0.0005
-0.0002  0.0028  1.0952  0.0005 -0.0001  0.0001
0.0019 -0.0007  0.0005  1.0919 -0.0011  0.0014
0.0002 -0.0004 -0.0001 -0.0011  1.0851  0.0030
0.0005 -0.0006  0.0001  0.0015  0.0031  1.0944
```

$K_v = 1.0e+004 *$

2.1108	0.0033	-0.0004	0.0015	0.0001	0.0004
0.0032	2.1175	0.0033	-0.0006	-0.0004	-0.0004
-0.0004	0.0032	2.1169	0.0004	-0.0001	0.0001
0.0015	-0.0007	0.0004	2.1145	-0.0009	0.0012
0.0001	-0.0004	-0.0001	-0.0009	2.1105	0.0025
0.0004	-0.0005	0.0001	0.0012	0.0025	2.1198

In the first simulation, effect of the system disturbance torque term τ_d is set to zero in order to validate the performance of Computed Torque Control based on the mathematical model.

Simulation 1: Computed Torque Control with Zero Disturbance

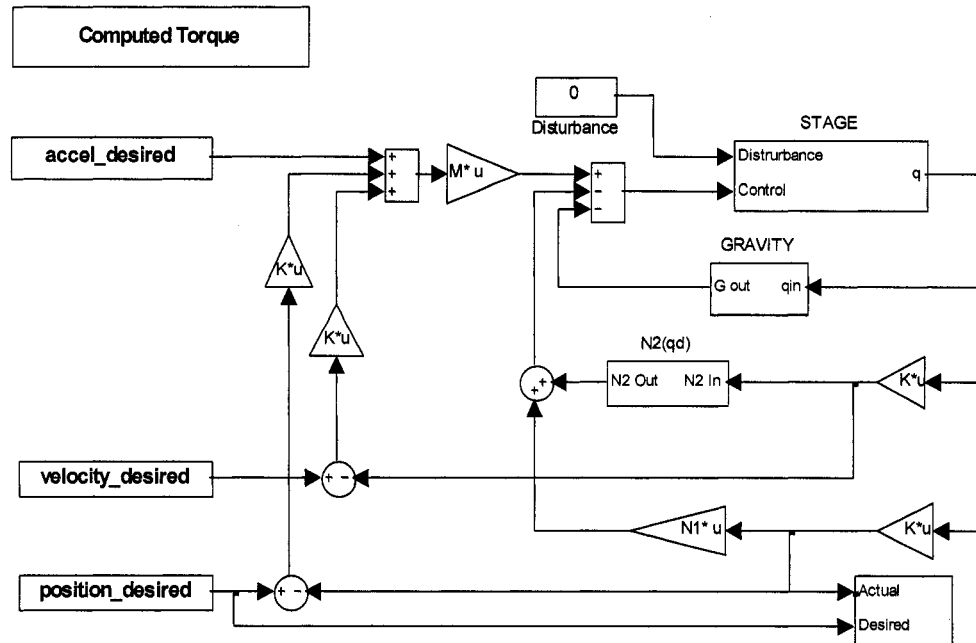


Fig. 16: Simulink Design of Computed Torque Control

The outputs of the three axes shown below:

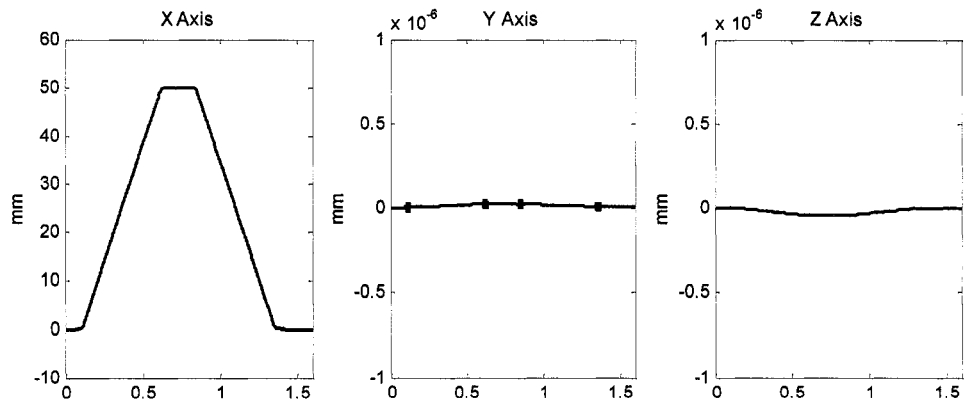


Fig. 17: Output of Computed Torque Control

In order to display the magnitude of the output, the x axis is scaled from -10mm to 60mm while the y and z axis are scaled in the range of $\pm 1e^{-6}\text{mm}$ or 1nm . The performance of Computed Torque Control can be evaluated from the position error plots shown below; all three axes are in the range of $\pm 10\text{nm}$.

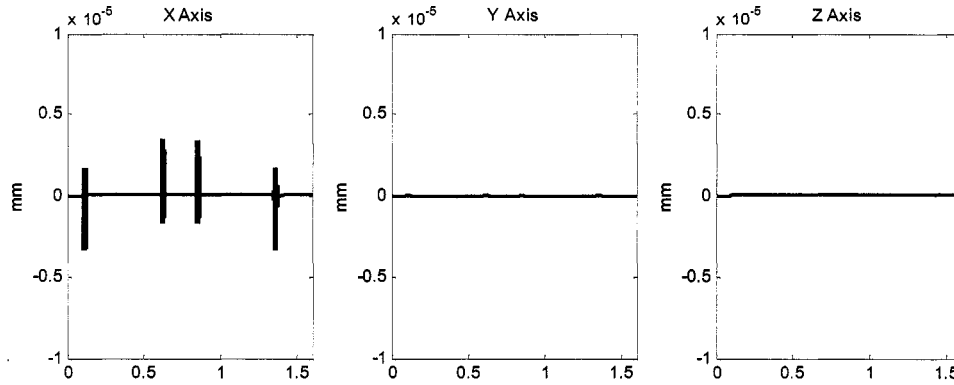


Fig. 18: Position Error of Computed Torque Control

Analyzing the error position by axis:

- X axis: The range of the error is within $\pm 3\text{nm}$, the maximum error is observed during the maximum acceleration phase. Gain parameters are tuned to reduce the error during the maximum acceleration, but it is not possible to achieve the range of error less than 3nm .
- Y axis: The range of the error is less than $\pm 1\text{nm}$; this is within the original specification.
- Z axis: The range of the error is less than $\pm 1\text{nm}$, satisfies the specification.

The overall performance of the control algorithm heavily depends on the rate of the acceleration, by reducing the rate of acceleration; Compute Torque Control can provide more robust performance.

Simulation 2: Large Disturbance on Computed Torque Control

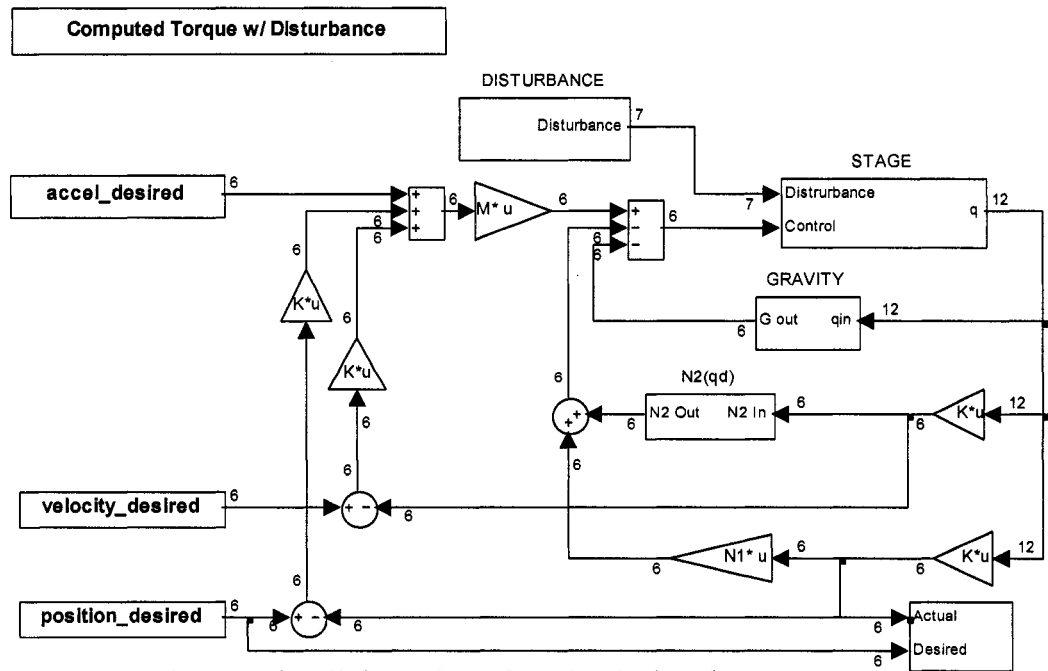


Fig. 19: Simulink Design of CTC w/ Disturbance

In this simulation, sine waves are added as disturbance torques to all six axes. Desired acceleration has the maximum acceleration peak of $4,000\text{mm/s}^2$ while the applied disturbance torque sine waves have the amplitude of 500gf/mm . The frequency of the disturbance signals are set at 10rad/s for the demonstration purpose.

The following plots display position errors on three axes scaled in $\pm 10\text{nm}$.

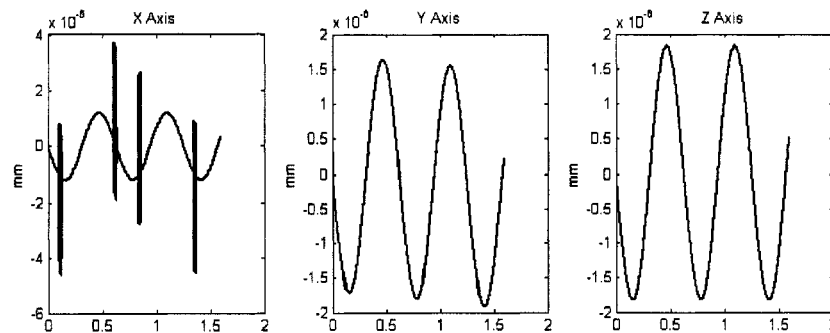


Fig. 20: Position Error of CTC w/ Disturbance

Analysis of disturbance effect on each axis:

- X axis: Clear indication of the disturbance effect on the position error, the maximum torque error is in phase with the sine wave, frequency of the disturbance is well preserved. Should the peak torque coincide with the sine wave, the magnitude of the position error will exceed far above 10nm.
- Y axis: It appears there is less disturbance effect on y axis compared to x axis, it is speculated that the system has a stiffer structure in the y axis than in the x axis based on the three leg design.
- Z axis: This axis has the most pronounced effect of the disturbance, the amplitude calculated in the z axis is larger than either the amplitude of error in the x or y axis. The system has three legs on the voice coils which provide a certain degree of damping which was not taken into consideration in the dynamic model; these damping forces may reduce the effect of the disturbance in the prototype simulation.

Generally, Computed Torque Control cannot effectively handle the disturbance since the control algorithm is based on the imperfect mathematical model. Disturbances not included in the mathematical model will certainly degrade the performance of the control.

The above simulation also proves that the z axis is rather sensitive to the disturbance; the actual system is designed to provide support from the three voice coils on the bottom through minus K^{TM} springs which provide constant forces rather than normal spring force relative the distance of the spring. Two magnetic coils on the x axis are also designed to provide the support in the z axis; however, the characteristics of the actuators in the x, y, and z axis are never established during the project by Ion Diagnostics.

The next simulation has the disturbance observer implemented on each of six axes to cancel the disturbance; the sine wave disturbance is maintained for this simulation to compare the performance of the controller. The subsequent simulation shows the performance of the controller given different types of disturbance other than the sine wave applied to the system.

Simulation 3: Disturbance Observer on Computed Torque Control

The disturbance observer is designed as:

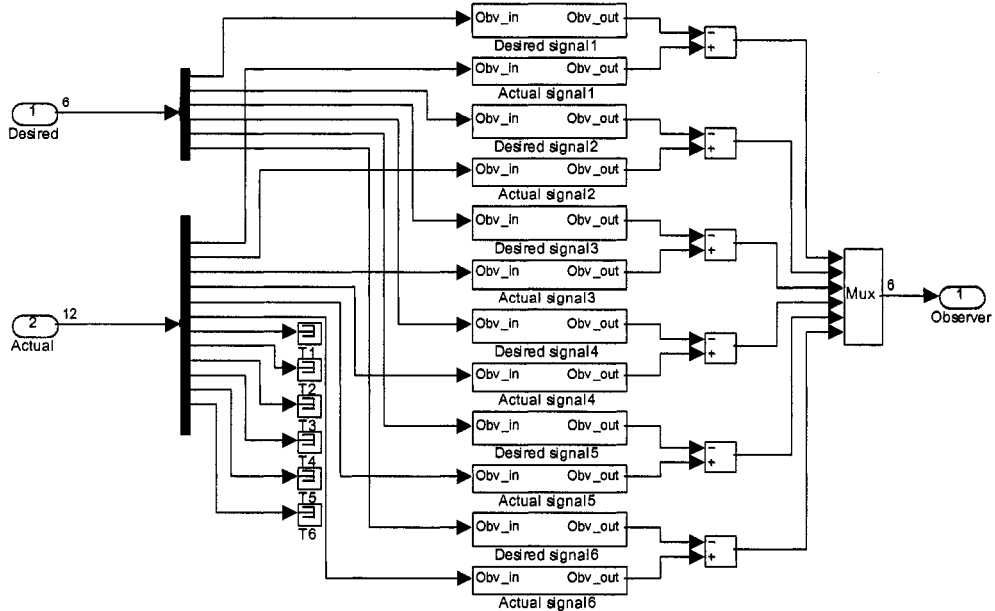


Fig. 21: Simulink Design of Disturbance Observer

the final Simulink design with disturbance observers on each axis is

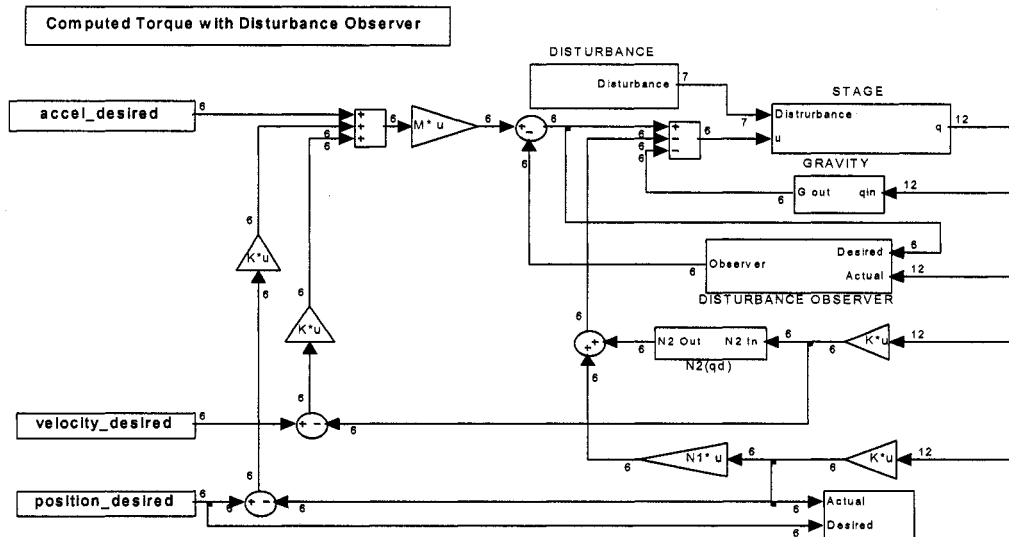


Fig. 22: Simulink Design of CTC with Disturbance Observer

Simulink yields the following position errors on six axes. (scaled $\pm 10\text{nm}$)

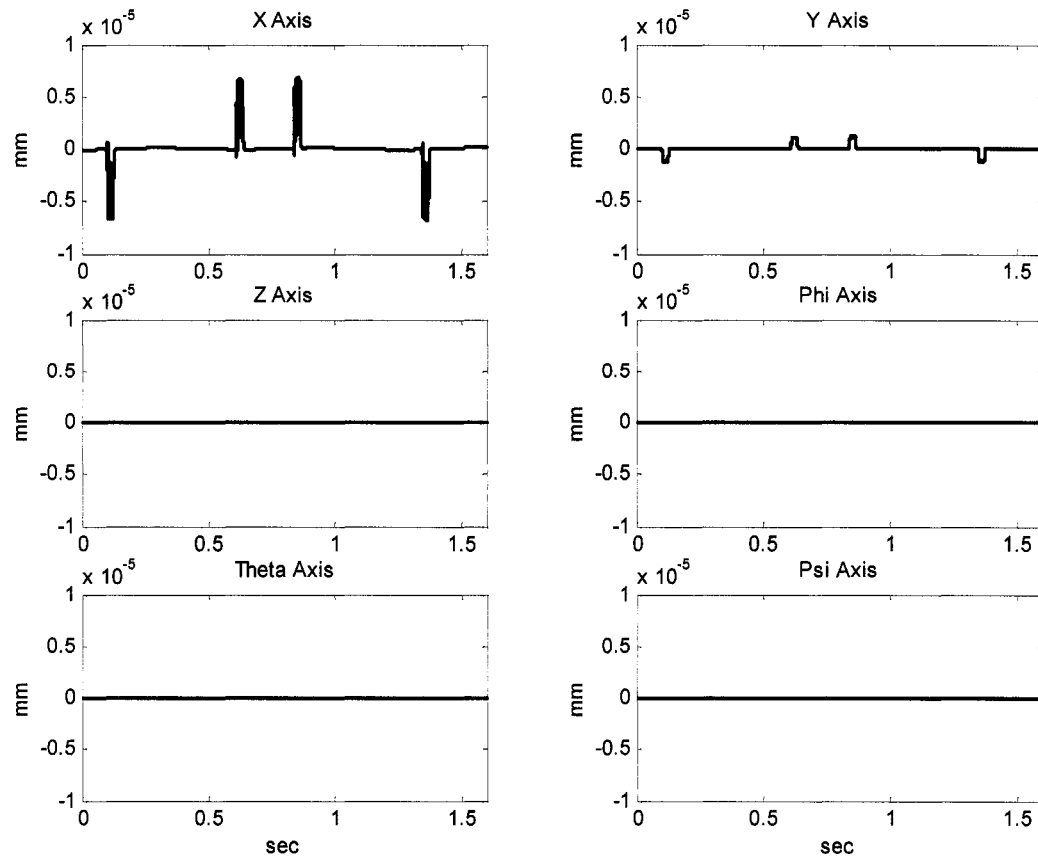


Fig. 23: Position Error of CTC with Disturbance Observer

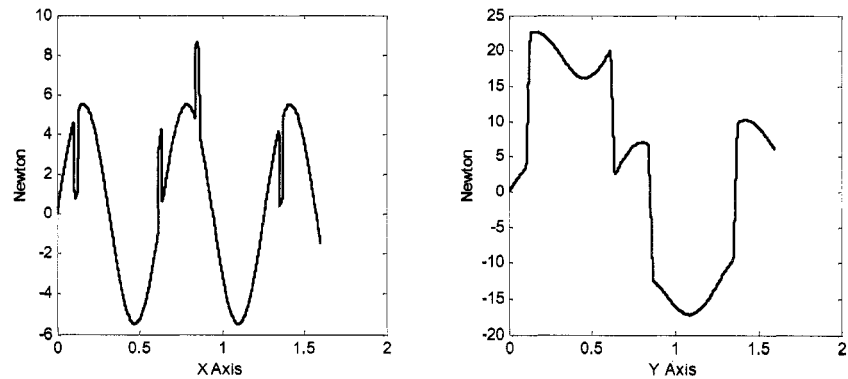
In all six axes, no trace of sine wave disturbances can be found. The disturbance observer has effectively cancelled the sine wave disturbances; however there is degradation of performance both in the x axis and y axis.

In Simulation 2 where disturbances is applied to Computed Torque Control without the disturbance observer, the position error is within $\pm 4\text{nm}$, however, when the disturbance observer is added to the controller, the range of the position error increases by the factor of 2, as large as $\pm 7\text{nm}$.

The basic theory of operation of the disturbance observer is to compare the actual signal against the desired signal; both signals are filtered through Q parameters. In this particular simulation a Butterworth filter design is employed. $Q(s)$ is defined such that 1 – $Q(s)$ has the frequency characteristic of a high pass filter.

Since there is one sample time delay between actual and desired signal, the performance of the disturbance observer can be tuned by adjusting the value of time delay, τ . The outputs of the disturbance observer for the x axis and the y axis are shown on the scopes below:

For $\tau = 0.001$



For $\tau = 0.00001$

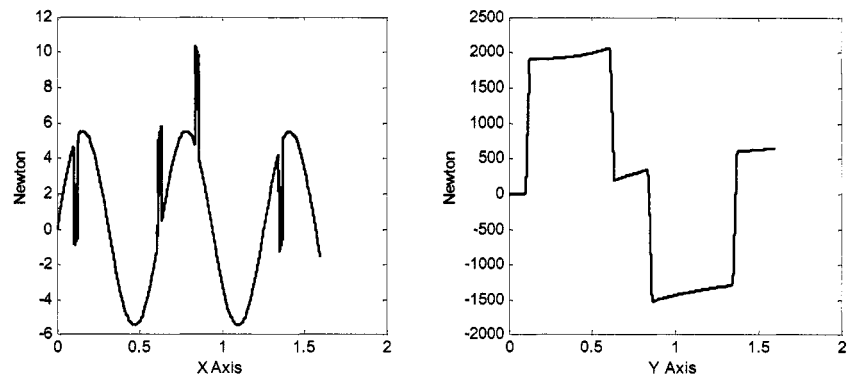


Fig. 24: Position Error of CTC w/ Disturbance Observer @ $\tau=0.001$

The output of the disturbance observer in the x axis is consistent while the output in the y axis had increased by 100 times.

The performance of the system with $\tau = 0.00001$:

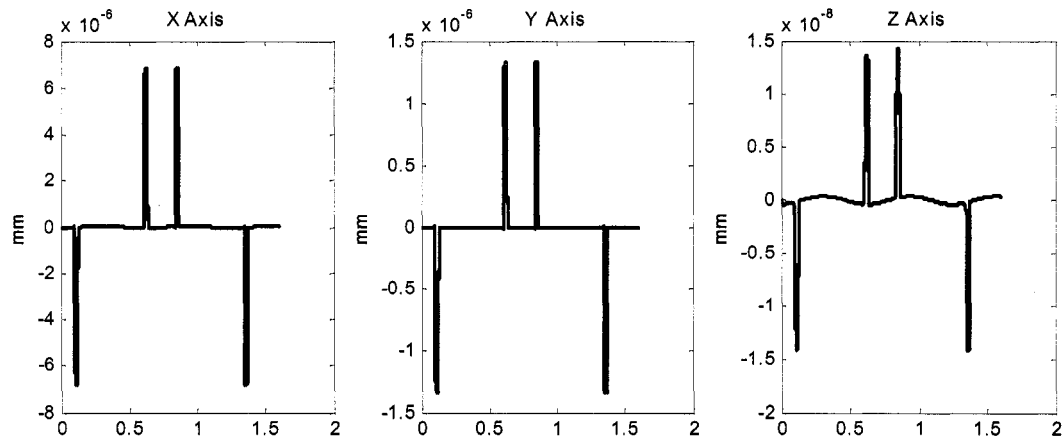


Fig. 25: Position Error of CTC w/ Disturbance Observer @ $\tau = 0.00001$

Apparently the disturbance observer perfectly cancels any trace of disturbance signals without affecting the performance of the system. However, there is a clear indication that this disturbance observer degrades the performance of Computed Torque Control while successfully canceling the disturbance noises. By analyzing the desired torque signal generated by Simulink, the cause of the degradation can be addressed.

Fundamentally, there is an inherent delay between the actual output and the desired input since the mathematical model compares the current desired input with the previous actual output. Any torque signals with the high rate of acceleration or deceleration will suffer from this delay effect of the disturbance observer. Furthermore, the information from the disturbance observer will be applied to adjust the value of the desired torque for the subsequent sample signal, therefore, there will be two sample time delays between the

actual output and the application of the disturbance signal to the system as illustrated below:

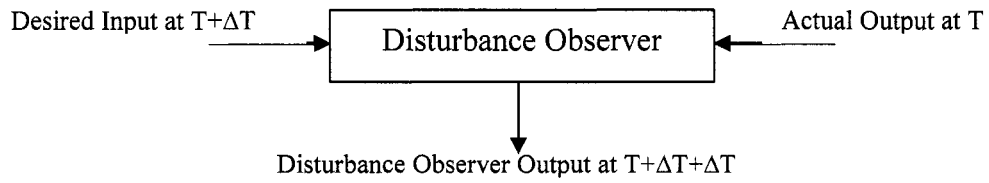


Fig. 26: Time Delay

It is evident that the disturbance observer generates the signal that reflects the time delays between the desired and actual output, which in turn degrades the performance of Computed Torque Control.

Conclusion

This research addresses two major issues:

1. Design of control algorithm for the multiple electronic beam stage.
2. Evaluation of performance of the disturbance observer in a multiple degrees of freedom system.

The physical characteristics of the stage are carefully analyzed, and then the dynamic equations are derived using La Grange and Euler method. The control algorithm is developed based on Computed Torque Control; robustness of the control is determined by the accuracy of the mathematic model generated. Due to the complexity of the stage design in addition to non-linearity of the system, it is not feasible to invest an extensive amount of time in developing an accurate mathematical model.

Dynamic equations are simplified and linearized, then converted to state space format to build a Matlab Simulink model, on which the control algorithm is validated. A simplified plant in state space dynamic equations format is used to tune Computed Torque Control, the performance of the control algorithm is within the specification originally targeted.

In order to compensate the terms eliminated during the simplification and linearization process, a disturbance observer is designed. Non linear terms and other eliminated terms are treated as disturbances to the system, and then the disturbances are applied to the system that is controlled by Computed Torque Control. This result is compared with the output of the system that has Computed Torque Control and the disturbance observer.

Computed Torque Control behaves poorly with the introduction of the disturbance; this supports the fact that the performance of Computed Torque Control heavily relies on the accuracy of the mathematical model. Introduction of any terms that affect the system will result in the degradation of the control since the control algorithm cannot effectively handle the inaccuracy of the model.

The disturbance observer added to Computed Torque Control significantly reduces the effect of the disturbance introduced to the system, virtually canceling any trace of a disturbance. However, this causes the degradation of the overall performance of the control of the system as the disturbance observer is suffering from the time delay between the desired and actual output. Regardless of numerous attempts made to minimize the time delay effect of the disturbance observer, the performance of the control system suffers from the time delay.

Computed Torque Control can provide excellent control performance if the mathematical model is accurate. The disturbance observer can be used to compensate for the inaccuracy in the mathematical model; however, the addition of the disturbance observer degrades the performance of Computed Torque Control while successfully handling the disturbance.

References

- Astrom, Karl Johan and Bjorn Wittermark. Adaptive Control. Boston: Addison Wesley, 1989.
- Etkin, Bernard. Dynamic of Flight: Stability and Control. New York: John Wiley & Sons Inc., 1982.
- Lewis, Frank, Chaouki T. Abdallah, and David M. Dawson. Control of Robot Manipulators. New York: Macmillan Publishing, 1993.
- Murakami, Toshiyuki. "A Motion Control Strategy Based on Equivalent Mass Matrix in Multidegree-of-Freedom Manipulator." IEEE Transactions on Industrial Electronics 42.2 (1995) : 123-130.
- Sciavicco, Lorenzo and Bruno Siciliano. Modeling and Control of Robot Manipulators. New York: McGraw-Hill Company, 1996.
- Tomizuka, Masayoshi. "Controller Structure for Robust High-Speed/High Accuracy Digital Motion Control." 1994 IEEE International Conference on Robotics and Automation (1994) : 1-18.
- Umeno, Takaji and Yoichi Hori. "Robust Speed Control of DC Servomotors Using Modern Two Degree-of-Freedom Controller Design." IEEE Transactions on Industrial Electronics 38.5 (1991) : 363-68.

Appendix 1

Values and Definition of Variables

Units: British Units (lbs, inches)

Inertial Tensor (physical value given by Solid Works)

$$I_{xx} \equiv \sum m_i (y_i^2 + z_i^2)$$

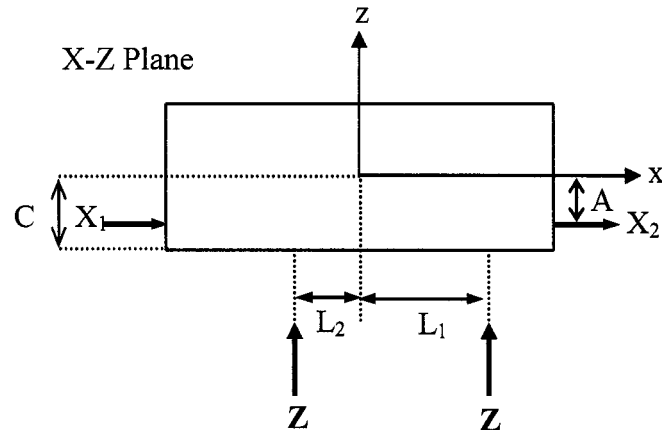
$$I_{yy} \equiv \sum m_i (z_i^2 + x_i^2)$$

$$I_{zz} \equiv \sum m_i (x_i^2 + y_i^2)$$

$$I_{xy} = I_{yx} \equiv -\sum m_i x_i y_i$$

$$I_{xz} = I_{zx} \equiv -\sum m_i x_i z_i$$

$$I_{yz} = I_{zy} \equiv -\sum m_i y_i z_i$$



$$g = (32.2 \text{ft/sec}^2) * 12$$

$$m = (1.32)/g \text{ (mass of leg) (unit: lb)}$$

$$M_s = (51.67 - (3 * m * g))/g \text{ (mass of stage w/o legs)}$$

(units: inches)

$$B = 1.503$$

$$c = 0.283$$

$$d = 5.4125$$

$$f = 15.07$$

$$H = 24.640$$

$$JJ = 3.380$$

$$k = 5.082$$

$$L1 = 3.1249$$

$$L2 = 2 * L1$$

$$I_o \equiv -\left(\frac{2I_{yy}}{H^2} + \frac{m}{2} \right)$$

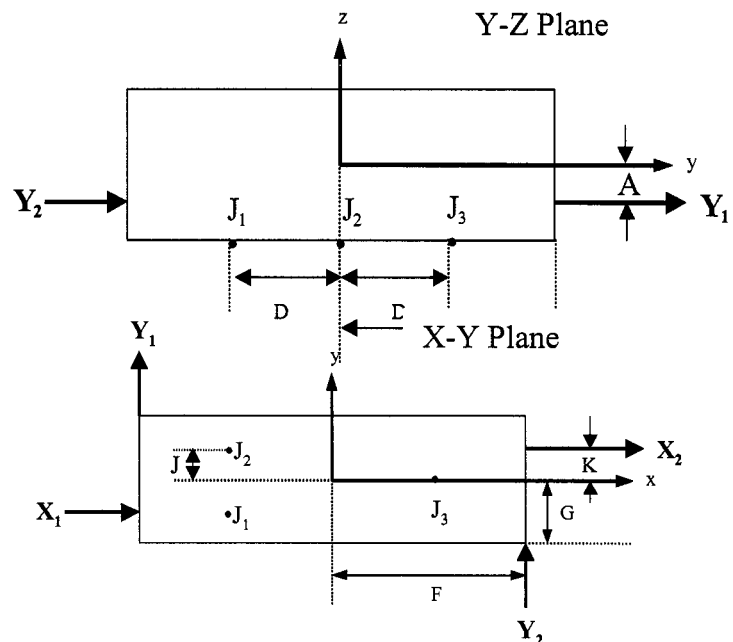


Fig. 27: Notations

Appendix 2

Dynamic Equations of Motion Derivation

The stage with three supporting legs is considered a multi-rigid-body dynamic system requiring two frames of reference in order to derive the dynamic equations.

The fixed inertia coordinate frame and the body coordinate frame are used to describe the position of the stage. The body coordinate frame is fixed on the stage body mass center that is time invariant with respect to the body coordinate frame.

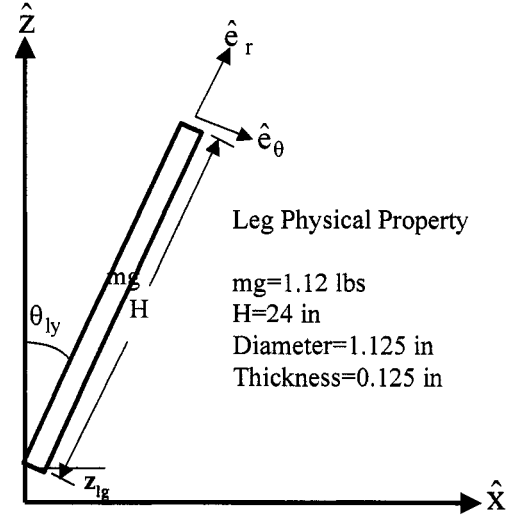


Fig. 28: Leg Physical Properties

The equation of the motion in the body coordinate frame is then transformed to the fixed inertia frame using the coordinate transformation matrix. The motion of the mass center of the stage and the orientation of the stage with respect to the fixed inertia frames are derived from the Euler's Equation of Motion.

Fig. 28 show two coordinate frames; fixed inertia frame $\hat{X} - \hat{Z}$ and body coordinate frame $\hat{e}_r - \hat{e}_\theta$, the transformation matrix is shown below.

Transformation Matrix

$$\begin{bmatrix} \hat{x} \\ \hat{z} \end{bmatrix} = \begin{bmatrix} \sin \theta_{ly} & \cos \theta_{ly} \\ \cos \theta_{ly} & -\sin \theta_{ly} \end{bmatrix} \begin{bmatrix} \hat{e}_r \\ \hat{e}_\theta \end{bmatrix} \quad \begin{bmatrix} \hat{e}_r \\ \hat{e}_\theta \end{bmatrix} = \begin{bmatrix} \sin \theta_{ly} & \cos \theta_{ly} \\ \cos \theta_{ly} & -\sin \theta_{ly} \end{bmatrix} \begin{bmatrix} \hat{x} \\ \hat{z} \end{bmatrix}$$

There are three legs supporting the whole weight of the stage translating forces in z direction from the voice coils supporting the legs. Fig. 28 describes the leg displacement and the physical property of the legs.

Kinematics

$$\vec{r}_G = z_{lg}\hat{z} + \frac{H}{2}\hat{e}_r = z_{lg}\hat{z} + \frac{H}{2}(\sin\theta_{ly}\hat{x} + \cos\theta_{ly}\hat{z}) = \frac{H}{2}\sin\theta_{ly}\hat{x} + \left(z_{lg} + \frac{H}{2}\cos\theta_{ly}\right)\hat{z}$$

$$\hat{V}_G = \dot{z}_{lg}\hat{z} + \dot{\theta}_{ly}\hat{e}_\theta \times \frac{H}{2}\hat{e}_r = \dot{z}_{lg}\hat{z} + \frac{H}{2}\dot{\theta}_{ly}\hat{e}_r$$

LaGrange's Equation

Kinetic Energy

$$\begin{aligned} T &= \frac{1}{2}mV_G^2 + \frac{1}{2}I_{yy}\dot{\theta}_{ly}^2 \\ &= \frac{1}{2}m\left[\left(\dot{z}_{lg}\hat{z} + \frac{H}{2}\dot{\theta}_{ly}\hat{e}_r\right) \cdot \left(\dot{z}_{lg}\hat{z} + \frac{H}{2}\dot{\theta}_{ly}\hat{e}_r\right)\right] + \frac{1}{2}I_{yy}\dot{\theta}_{ly}^2 \\ &= \frac{1}{2}m\left(\dot{z}_{lg}^2 + \frac{H^2}{4}\dot{\theta}_{ly}^2\right) + \frac{1}{2}I_{yy}\dot{\theta}_{ly}^2 \\ &= \frac{1}{2}m\dot{z}_{ly}^2 + \frac{1}{2}\left(I_{yy} + \frac{H^2}{4}m\right)\dot{\theta}_{ly}^2 \end{aligned}$$

Potential Energy

$$U = mg\left(\frac{H}{2}\cos\theta_{ly}\right) + mgz_{lg} = mg\left(\frac{H}{2}\cos\theta_{ly} + z_{lg}\right)$$

Generalized Forces

$$Q_\theta = \frac{H}{2}\sin\theta_{ly}Z - F_x \frac{H}{2}$$

$$Q_Z = Z + F_x\sin\theta_{ly} - F_z\cos\theta_{ly} - Kz_{lg}$$

Minus K spring allows Kz_{lg} to be constant; then, the force from Kz_{lg} can be included in Z .

Since $L \equiv T - U$

$$= \frac{1}{2}m\dot{z}_{lg}^2 + \frac{1}{2}\left(I_{yy} + \frac{H^2}{4}m\right)\dot{\theta}_{ly}^2 - mg\left(\frac{H}{2}\cos\theta_{ly} + z_{lg}\right)$$

For all generalized coordinates

$$\frac{d}{dt} \left(\frac{\partial L}{\partial \dot{q}_i} \right) - \frac{\partial L}{\partial q_i} = Q_i$$

in z - coordinate

$$\frac{\partial L}{\partial z} = -mg \qquad \frac{\partial L}{\partial \dot{z}} = m\dot{z}_{1g} \qquad \frac{d}{dt} \left(\frac{\partial L}{\partial \dot{z}} \right) = m\ddot{z}_{1g}$$

in θ_{1y} - coordinate

$$\frac{\partial L}{\partial \theta_{1y}} = \frac{H}{2} mg \sin \theta_{1y} \qquad \frac{\partial L}{\partial \dot{\theta}_{1y}} = \left(I_{yy} + \frac{H^2}{4} m \right) \dot{\theta}_{1y} \qquad \frac{d}{dt} \left(\frac{\partial L}{\partial \dot{\theta}_{1y}} \right) = \left(I_{yy} + \frac{H^2}{4} m \right) \ddot{\theta}_{1y}$$

Equation of motion can be expressed in terms of

$$\begin{aligned} Z : \quad m\ddot{z}_{1g} + mg &= Z + F_x \sin \theta_{1y} - F_z \cos \theta_{1y} \\ \theta_{1y} : \quad \left(I_{yy} + \frac{H^2}{4} m \right) \ddot{\theta}_{1y} - \frac{H}{2} mg \sin \theta_{1y} &= \frac{H}{2} \sin \theta_{1y} Z - \frac{H}{2} F_x \end{aligned}$$

Now, F_x and F_z can be found

$$\begin{aligned} \frac{H}{2} F_x &= - \left(I_{yy} + \frac{H^2}{4} m \right) \ddot{\theta}_{1y} + \frac{H}{2} mg \sin \theta_{1y} + \frac{H}{2} \sin \theta_{1y} Z \\ F_x &= - \left(\frac{2I_{yy}}{H} + \frac{H}{2} m \right) \ddot{\theta}_{1y} + (mg + Z) \sin \theta_{1y} \\ F_z \cos \theta_{1y} &= Z + F_x \sin \theta_{1y} - m\ddot{z}_{1g} - mg \\ &= Z + \left[- \left(\frac{2I_{yy}}{H} + \frac{H}{2} m \right) \ddot{\theta}_{1y} + (mg + Z) \sin \theta_{1y} \right] \sin \theta_{1y} - m\ddot{z}_{1g} - mg \\ F_z &= \frac{- \left(\frac{2I_{yy}}{H} + \frac{H}{2} m \right) \ddot{\theta}_{1y} \sin \theta_{1y} - m\ddot{z}_{1g} + Z(1 + \sin^2 \theta_{1y}) + mg(\sin^2 \theta_{1y} - 1)}{\cos \theta_{1y}} \end{aligned}$$

This equation can be linearized and simplified

$$F_z = - \left(\frac{2I_{yy}}{H} + \frac{H}{2} m \right) \ddot{\theta}_{1y} \theta_{1y} - m\ddot{z}_{1g} + Z - mg = Z - m\ddot{z}_{1g} - mg + NL_a$$

$$\text{where } NLa = -\left(\frac{2I_{yy}}{H} + \frac{H}{2}m\right)\ddot{\theta}_{1y}\theta_{1y}$$

Leg angles θ and ϕ , and displacement z can be expressed in the stage coordinate system

Leg#1

$$\begin{aligned}\theta_{1y} &= \frac{x - L_2\theta}{H} & \phi_{1x} &= \frac{y + D\phi}{H} & z_{1g} &= z + L_2\theta - D\phi \\ \dot{\theta}_{1y} &= \frac{\dot{x} - L_2\dot{\theta}}{H} & \dot{\phi}_{1x} &= \frac{\dot{y} + D\dot{\phi}}{H} & \dot{z}_{1g} &= \dot{z} + L_2\dot{\theta} - D\dot{\phi} \\ \ddot{\theta}_{1y} &= \frac{\ddot{x} - L_2\ddot{\theta}}{H} & \ddot{\phi}_{1x} &= \frac{\ddot{y} + D\ddot{\phi}}{H} & \ddot{z}_{1g} &= \ddot{z} + L_2\ddot{\theta} - D\ddot{\phi}\end{aligned}$$

Leg#2

$$\begin{aligned}\theta_{1y} &= \frac{x - L_2\theta}{H} & \phi_{1x} &= \frac{y + D\phi}{H} & z_{1g} &= z + L_2\theta + D\phi \\ \dot{\theta}_{1y} &= \frac{\dot{x} - L_2\dot{\theta}}{H} & \dot{\phi}_{1x} &= \frac{\dot{y} + D\dot{\phi}}{H} & \dot{z}_{1g} &= \dot{z} + L_2\dot{\theta} + D\dot{\phi} \\ \ddot{\theta}_{1y} &= \frac{\ddot{x} - L_2\ddot{\theta}}{H} & \ddot{\phi}_{1x} &= \frac{\ddot{y} + D\ddot{\phi}}{H} & \ddot{z}_{1g} &= \ddot{z} + L_2\ddot{\theta} + D\ddot{\phi}\end{aligned}$$

Leg#3

$$\begin{aligned}\theta_{1y} &= \frac{x - L_1\theta}{H} & \phi_{1x} &= \frac{y + D\phi}{H} & z_{1g} &= z - L_1\theta \\ \dot{\theta}_{1y} &= \frac{\dot{x} - L_1\dot{\theta}}{H} & \dot{\phi}_{1x} &= \frac{\dot{y} + D\dot{\phi}}{H} & \dot{z}_{1g} &= \dot{z} - L_1\dot{\theta} \\ \ddot{\theta}_{1y} &= \frac{\ddot{x} - L_1\ddot{\theta}}{H} & \ddot{\phi}_{1x} &= \frac{\ddot{y} + D\ddot{\phi}}{H} & \ddot{z}_{1g} &= \ddot{z} - L_1\ddot{\theta}\end{aligned}$$

Note that $L_2=2xL_1$

Forces supporting the stage, F_x , F_y , and F_z can be linearized and expressed as,

$$\begin{aligned}F_x &= -\left(\frac{2I_{yy}}{H} + \frac{H}{2}m\right)\ddot{\theta}_{1y} + (mg + Z)\sin\theta_{1y} \\ &= -\left(\frac{2I_{yy}}{H} + \frac{H}{2}m\right)\left(\frac{\ddot{x} - L_2\ddot{\theta}}{H}\right) + (mg + Z)\left(\frac{x - L_2\theta}{H}\right) \\ &= -\left(\frac{2I_{yy}}{H^2} + \frac{m}{2}\right)(\ddot{x} - L_2\ddot{\theta}) + \left(\frac{mg}{H} + \frac{Z}{H}\right)(x - L_2\theta)\end{aligned}$$

$$\text{Let } I_o \equiv -\left(\frac{2I_{yy}}{H^2} + \frac{m}{2}\right)$$

$$\therefore F_x = I_o(\ddot{x} - L_2\ddot{\theta}) + \frac{1}{H}(mg + Z)(x - L_2\theta)$$

$$\text{Leg\#1 } F_{x1} = I_o(\ddot{x} - L_2\ddot{\theta}) + \frac{1}{H}(mg + Z_1)(x - L_2\theta)$$

$$\text{Leg\#2 } F_{x2} = I_o(\ddot{x} - L_2\ddot{\theta}) + \frac{1}{H}(mg + Z_2)(x - L_2\theta)$$

$$\text{Leg\#3 } F_{x3} = I_o(\ddot{x} - L_1\ddot{\theta}) + \frac{1}{H}(mg + Z_3)(x - L_1\theta)$$

For a cylindrical bar, $I_{xx} = I_{yy}$, then same analogy can be applied to obtain F_y for all 3 legs.

$$\begin{aligned} F_y &= -\left(\frac{2I_{xx}}{H^2} + \frac{m}{2}\right)\ddot{\phi}_{1x} + (mg + Z)\sin\phi_{1x} \\ &= I_o\ddot{\phi}_{1x} + (mg + Z)\sin\phi_{1x} \\ &= I_o(\ddot{y} + D\ddot{\phi}) + \frac{1}{H}(mg + Z)(y + D\phi) \end{aligned}$$

$$\text{Leg\#1 } F_{y1} = I_o(\ddot{y} + D\ddot{\phi}) + \frac{1}{H}(mg + Z_1)(y + D\phi)$$

$$\text{Leg\#2 } F_{y2} = I_o(\ddot{y} + D\ddot{\phi}) + \frac{1}{H}(mg + Z_2)(y + D\phi)$$

$$\text{Leg\#3 } F_{y3} = I_o(\ddot{y} + D\ddot{\phi}) + \frac{1}{H}(mg + Z_3)(y + D\phi)$$

F_z to be obtained as follows,

$$F_z = Z - m\ddot{z}_{1g} - mg + NLa$$

$$\text{Leg\#1 } F_{z1} = Z_1 - m(\ddot{z} + L_2\ddot{\theta} - D\ddot{\phi}) - mg + NLa_1$$

$$\text{Leg\#2 } F_{z2} = Z_2 - m(\ddot{z} + L_2\ddot{\theta} + D\ddot{\phi}) - mg + NLa_2$$

$$\text{Leg\#3 } F_{z3} = Z_3 - m(\ddot{z} - L_1\ddot{\theta}) - mg + NLa_3$$

NLa_1 , NLa_2 , and NLa_3 to be discussed later

External Forces and Moments

$$X = -(F_{x1} + F_{x2} + F_{x3}) + X_1 + X_2 \quad X_1 \text{ and } X_2 : \text{External forces from magnetic motors}$$

$$Y = -(F_{y1} + F_{y2} + F_{y3}) + Y_1 + Y_2 \quad Y_1 \text{ and } Y_2 : \text{External forces from magnetic motors}$$

$$Z = F_{z1} + F_{z2} + F_{z3}$$

$$L = (Y_1 + Y_2)A + (F_{z2} - F_{z1})D - (F_{y1} + F_{y2} + F_{y3})C$$

$$M = (F_{x1} + F_{x2} + F_{x3})C - F_{z3}L_1 + (F_{z1} + F_{z2})L_2 - (X_1 + X_2)A$$

$$N = (F_{x2} - F_{x1})J - F_{y3}L_1 + (F_{y1} + F_{y2})L_2 - (x_1 - x_2)K + (Y_2 - Y_1)F$$

3 external forces and 3 moments are described as:

$$\begin{aligned} X &= -(F_{x1} + F_{x2} + F_{x3}) + X_1 + X_2 \\ &= -I_0(\ddot{x} - L_2\ddot{\theta}) + \frac{1}{H}(mg + Z_1)(x - L_2\theta) + I_0(\ddot{x} - L_2\ddot{\theta}) + \frac{1}{H}(mg + Z_2)(x - L_2\theta) \\ &\quad + I_0(\ddot{x} - L_1\ddot{\theta}) + \frac{1}{H}(mg + Z_3)(x - L_1\theta) + X_1 + X_2 \\ &= -[3I_0\ddot{x} - 3L_1\ddot{\theta} + \frac{3mg}{H}x + \frac{9mgL_1}{H}\theta + \frac{1}{H}(Z_1 + Z_2 + Z_3)x - \\ &\quad \frac{1}{H}(L_2Z_1 + L_2Z_2 + L_1Z_3)\theta] + X_1 + X_2 \end{aligned}$$

$$\begin{aligned} Y &= -(F_{y1} + F_{y2} + F_{y3}) + Y_1 + Y_2 \\ &= -[I_0(\ddot{y} + D\ddot{\phi}) + \frac{1}{H}(mg + Z_1)(y + D\phi) + I_0(\ddot{y} + D\ddot{\phi}) + \frac{1}{H}(mg + Z_2)(y + D\phi) \\ &\quad + I_0(\ddot{y} + D\ddot{\phi}) + \frac{1}{H}(mg + Z_3)(y + D\phi)] + Y_1 + Y_2 \\ &= -\left[3I_0\ddot{y} + 3I_0D\ddot{\phi} + \frac{3mg}{H}(y + D\phi) + \frac{1}{H}(Z_1 + Z_2 + Z_3)(y + D\phi)\right] + Y_1 + Y_2 \end{aligned}$$

$$\begin{aligned} Z &= F_{z1} + F_{z2} + F_{z3} \\ &= (Z_1 + Z_2 + Z_3) - 3m\ddot{z} - 5mL_1\ddot{\theta} - 3mg + NLa_1 + NLa_2 + NLa_3 \end{aligned}$$

$$\begin{aligned}
L &= (Y_1 + Y_2)A + (F_{z2} - F_{z1})D - (F_{y1} + F_{y2} + F_{y3})C \\
&= (Y_1 + Y_2)A - 2D^2 m\ddot{\phi} + (NLa_2 - NLa_1)D \\
&\quad - \left[3I_o \ddot{y} + 3I_o D\ddot{\phi} + \frac{3mg}{H}(y + D\phi) + \frac{1}{H}(Z_1 + Z_2 + Z_3)(y + D\phi) \right] C
\end{aligned}$$

$$\begin{aligned}
M &= (F_{x1} + F_{x2} + F_{x3})C - F_{z3}L_1 + (F_{z1} + F_{z2})L_2 - (X_1 + X_2)A \\
&= \left[3I_o \ddot{x} - 3I_o L_1 \ddot{\theta} + \frac{3mg}{H}x + \frac{9mgL_1}{H}\theta + \frac{1}{H}(Z_1 + Z_2 + Z_3)x \right. \\
&\quad \left. - \frac{1}{H}(L_2 Z_1 + L_2 Z_2 + L_1 Z_3)\theta \right] C - \left[Z_3 - m(\ddot{z} - L_1 \ddot{\theta}) - mg + NLa_3 \right] L_1 \\
&\quad + \left[(Z_1 + Z_2) - 2m(\ddot{z} + L_2 \ddot{\theta}) - 2mg + NLa_1 + NLa_2 \right] L_2 - (X_1 + X_2)A \\
&= 3I_o C \ddot{x} - I_o (2L_2 - L_1) C \ddot{\theta} + \frac{3mgC}{H}x - \frac{9mgL_1 C}{H}\theta + \frac{C}{H}(Z_1 + Z_2 + Z_3)x \\
&\quad - \frac{C}{H}(L_2 Z_1 + L_2 Z_2 + L_1 Z_3)\theta - L_1 Z_3 + (Z_1 + Z_2)L_2 - (mL_1 + 2mL_2)\ddot{z} \\
&\quad + (mL_1^2 - 2mL_2^2)\ddot{\theta} - 3L_1 mg + L_1 NLa_3 + L_2 (NLa_1 + NLa_2)
\end{aligned}$$

$$\begin{aligned}
N &= (F_{x2} - F_{x1})J - F_{y3}L_1 + (F_{y1} + F_{y2})L_2 - (X_1 - X_2)K + (Y_2 - Y_1)F \\
&= (0)J + \left[I_o (\ddot{y} + D\ddot{\phi}) + \frac{1}{H}(mg + Z_3)(y + D\phi) \right] (2L_2 - L_1) - (X_1 - X_2)K + (Y_2 - Y_1)F \\
&= 3I_o L_1 \ddot{y} + 3I_o D L_1 \ddot{\phi} + \frac{3L_1}{H}mgy + \frac{3L_1}{H}mgD\phi \\
&\quad + \frac{3Z_3 L_1}{H}(y + D\phi) - (X_1 - X_2)K + (Y_2 - Y_1)F
\end{aligned}$$

Magnetic forces $X_1, X_2, Y_1, Y_2, Z_1, Z_2$ and Z_3 can be obtained using Euler's equation.

Euler's Equations

Pitch, roll, and yaw angle of an object in 3-D can be described by Euler angles. Utilizing this concept, Dynamics of Flight by B. Etkin provides necessary equations with all the coupling terms already derived as shown below:

Terminology:

A, B, C	moments of inertia about (x,y,z) axes
D, E, F	products of inertia
L, M, N	scalar components of resultant external moment vector about the mass center
P, Q, R	scalar components of angular velocity vector
U, V, W	scalar components of velocity vector
X, Y, Z	components of resultant forces acting on the object
ψ, θ, ϕ	Euler angles
M_s	mass of stage
m	mass of one leg

Equations: (Modified to reflect Ion's coordinate system)

$$\begin{aligned} X + M_s g \sin \theta &= M_s (\dot{U} + QW - RV) \\ Y - M_s g \cos \theta \cos \theta &= M_s (\dot{V} + RU - PW) \\ Z - (M_s + 3m) g \cos \theta \cos \theta &= M_s (\dot{W} + PV - QU) \end{aligned}$$

$$\begin{aligned} L &= I_{xx} \dot{P} - I_{xz} \dot{R} + (I_{zz} - I_{yy}) QR - I_{xz} PQ \\ M &= I_{yy} \dot{Q} + (I_{xx} - I_{zz}) RP + I_{xz} (P^2 - R^2) \\ N &= -I_{xz} \dot{P} + I_{zz} \dot{R} + (I_{yy} - I_{xx}) PQ + I_{xz} QR \end{aligned}$$

$$\begin{aligned} P &= \dot{\phi} - \dot{\psi} \sin \theta \\ Q &= \dot{\theta} \cos \phi + \dot{\psi} \cos \theta \sin \theta \\ R &= \dot{\psi} \cos \theta \sin \theta - \dot{\theta} \sin \phi \\ \dot{\theta} &= Q \cos \phi - R \sin \phi \\ \dot{\phi} &= P + Q \sin \phi \sin \theta + R \cos \phi \cos \theta \end{aligned}$$

$$\dot{\psi} = (Q\sin\phi + R\cos\phi)\sec\theta$$

$$\frac{dx'}{dt} = U\cos\theta\cos\theta + V(\sin\phi\sin\psi - \cos\phi\cos\psi) + W(\cos\phi\sin\psi + \sin\phi\cos\psi)$$

$$\frac{dy'}{dt} = U\cos\theta\sin\theta + V(\sin\phi\cos\psi + \cos\phi\sin\psi) + W(\cos\phi\cos\psi - \sin\phi\sin\psi)$$

$$\frac{dz'}{dt} = U\sin\theta + V\sin\phi\sin\psi + W\cos\phi\cos\psi$$

Evidently, forces and moments are coupled barring from building any potentially realizable mathematical modeling. The following steps are necessary to decouple forces and moments in order to build a mathematical model.

$$X + M_s g \sin\theta = M_s (\dot{U} + QW - RV)$$

$$X = M_s (\dot{U} + QW - RV) - M_s g \sin\theta$$

$$\begin{aligned} &= M_s [\ddot{x} + (\dot{\theta}\cos\phi + \dot{\psi}\cos\theta\sin\phi)\dot{z} - (\dot{\psi}\cos\theta\sin\phi - \dot{\theta}\sin\phi)\dot{y}] - M_s g \sin\theta \\ &= M_s (\ddot{x} + \dot{\theta}\dot{z} - \dot{\psi}\dot{y}) - M_s g \sin\theta \\ &\quad - \left[3I_o \ddot{x} - 3I_o L_1 \ddot{\theta} + \frac{3mg}{H} x + \frac{9mgL_1}{H} \theta + \frac{1}{H} (Z_1 + Z_2 + Z_3) x \right. \\ &\quad \left. - \frac{1}{H} (L_2 Z_1 + L_2 Z_2 + L_1 Z_3) \theta \right] + x_1 + x_2 \\ &= M_s (\ddot{x} + \dot{\theta}\dot{z} - \dot{\psi}\dot{y}) - M_s g \sin\theta \end{aligned}$$

$$\begin{aligned} X_1 + X_2 &= (3I_o + M_s) \ddot{x} - 3I_o L_1 \ddot{\theta} + \frac{3mg}{H} x + \frac{9mgL_1}{H} \theta - M_s g \sin\theta + \\ &\quad \frac{1}{H} (Z_1 + Z_2 + Z_3) x - \frac{1}{H} (L_2 Z_1 + L_2 Z_2 + L_1 Z_3) \theta + M_s (\dot{\theta}\dot{z} - \dot{\psi}\dot{y}) \end{aligned}$$

$$\begin{aligned}
Y - M_s g \cos \theta \cos \theta &= M_s (\dot{V} + RU - PW) \\
&= M_s (\ddot{y} + \dot{\psi} \dot{x} - \dot{\phi} \dot{z}) \\
&- \left[3I_o \ddot{y} + 3I_o D \ddot{\phi} + \frac{3mg}{H} (y + D\phi) + \frac{1}{H} (Z_1 + Z_2 + Z_3) (y + D\phi) \right] + Y_1 + Y_2 \\
&= M_s (\ddot{y} + \dot{\psi} \dot{x} - \dot{\phi} \dot{z}) + M_s g \cos \theta \cos \theta
\end{aligned}$$

$$\begin{aligned}
Y_1 + Y_2 &= (3I_o + M_s) \ddot{y} + 3I_o D \ddot{\phi} + \frac{3mg}{H} y + \frac{3mgD}{H} \phi + \frac{1}{H} (Z_1 + Z_2 + Z_3) y \\
&+ \frac{1}{H} (Z_1 + Z_2 + Z_3) D \phi + M_s g \cos \theta \cos \theta + M_s (\dot{\psi} \dot{x} - \dot{\phi} \dot{z})
\end{aligned}$$

$$\begin{aligned}
z - (M_s + 3m) g \cos \theta \cos \theta &= M_s (\dot{W} + PV - QU) \\
&= M_s (\ddot{z} + \dot{\phi} \dot{y} - \dot{\theta} \dot{z})
\end{aligned}$$

$$\begin{aligned}
(Z_1 + Z_2 + Z_3) - 3m\ddot{z} - 5mL_1 \ddot{\theta} - 3mg + NLa_T - (M_s + 3m) g \cos \theta \cos \theta \\
= M_s (\ddot{z} + \dot{\phi} \dot{y} - \dot{\theta} \dot{z})
\end{aligned}$$

$$\text{where } NLa_T = NLa_1 + NLa_2 + NLa_3$$

$$\begin{aligned}
Z_1 + Z_2 + Z_3 &= (M_s + 3m) \ddot{z} + 5mL_1 \ddot{\theta} + 3mg + (M_s + 3m) g \cos \theta \cos \theta \\
&+ M_s (\dot{\phi} \dot{y} - \dot{\theta} \dot{z}) - NLa_T
\end{aligned}$$

$$\begin{aligned}
L &= I_{s_{xx}} \dot{P} - I_{s_{xz}} \dot{R} + (I_{s_{zz}} - I_{s_{yy}}) QR - I_{s_{xz}} PQ \\
&= I_{s_{xx}} \ddot{\phi} - I_{s_{xz}} \ddot{\psi} + (I_{s_{zz}} - I_{s_{yy}}) \dot{\theta} \dot{\psi} - I_{s_{xz}} \dot{\phi} \dot{\theta}
\end{aligned}$$

$$\begin{aligned}
(Y_1 + Y_2)A - 2D^2 m \ddot{\phi} + (NLa_2 - NLa_1)D - 3I_o C \ddot{y} - 3I_o CD \ddot{\phi} - \frac{3mgC}{H} y - \frac{3mgC}{H} \phi \\
- \frac{C}{H} (Z_1 + Z_2 + Z_3) y - \frac{DC}{H} (Z_1 + Z_2 + Z_3) \phi = I_{s_{xx}} \ddot{\phi} - I_{s_{xz}} \ddot{\psi} + (I_{s_{zz}} - I_{s_{yy}}) \dot{\theta} \dot{\psi} - I_{s_{xz}} \dot{\phi} \dot{\theta}
\end{aligned}$$

$$\begin{aligned}
(Y_1 + Y_2)A &= 3I_o C \ddot{y} + (3I_o CD + 2D^2 m + I_{s_{xx}}) \ddot{\phi} - I_{s_{xz}} \ddot{\psi} + \frac{3mgC}{H} y + \frac{3mgCD}{H} \phi \\
&+ \frac{C}{H} (Z_1 + Z_2 + Z_3) y + \frac{DC}{H} (Z_1 + Z_2 + Z_3) \phi + (I_{s_{zz}} - I_{s_{yy}}) \dot{\theta} \dot{\psi} - I_{s_{xz}} \dot{\phi} \dot{\theta} - (NLa_2 - NLa_1)D
\end{aligned}$$

$$\begin{aligned} M &= I_{s_{yy}} \dot{Q} + (I_{s_{xx}} - I_{s_{zz}}) RP + I_{s_{xz}} (P^2 - R^2) \\ &= I_{s_{yy}} \ddot{\theta} + (I_{s_{xx}} - I_{s_{zz}}) \dot{\psi} \dot{\phi} + I_{s_{xz}} (\dot{\phi}^2 - \dot{\psi}^2) \end{aligned}$$

$$\begin{aligned} &3I_o C \ddot{x} - 3I_o L_1 C \ddot{\theta} + \frac{3mgC}{H} x + \frac{9mgCL_1}{H} \theta + \frac{C}{H} (Z_1 + Z_2 + Z_3) x \\ &- \frac{C}{H} (L_2 Z_1 + L_2 Z_2 + L_1 Z_3) \theta - L_1 Z_3 + (Z_2 + Z_3) L_2 - m(L_1 + 2L_2) \ddot{z} \\ &- 3mL_1^2 \ddot{\theta} - 3L_1 mg + L_1 NLa_3 + L_2 (NLa_1 + NLa_2) \\ &= I_{s_{yy}} \ddot{\theta} + (I_{s_{xx}} - I_{s_{zz}}) \dot{\psi} \dot{\phi} + I_{s_{xz}} (\dot{\phi}^2 - \dot{\psi}^2) \end{aligned}$$

$$\begin{aligned} (Z_1 + Z_2) L_2 - L_1 Z_3 &= -3I_o C \ddot{x} + 5mL_1 \ddot{z} + [3I_o L_1 C - 3mL_1^2 + I_{s_{yy}}] \ddot{\theta} \\ &- \frac{3mgC}{H} x - \frac{9mgCL_1}{H} \theta + 3L_1 mg + (I_{s_{xx}} - I_{s_{zz}}) \dot{\psi} \dot{\phi} + I_{s_{xz}} (\dot{\phi}^2 - \dot{\psi}^2) - \frac{C}{H} (Z_1 + Z_2 + Z_3) x \\ &+ \frac{C}{H} (L_2 Z_1 + L_2 Z_2 + L_1 Z_3) \theta - L_1 NLa_3 + L_2 (NLa_1 + NLa_2) \end{aligned}$$

$$\begin{aligned} N &= -I_{s_{xz}} \dot{P} + I_{s_{zz}} \dot{R} + (I_{s_{yy}} - I_{s_{xx}}) PQ + I_{s_{xz}} QR \\ &= -I_{s_{xz}} \ddot{\phi} + I_{s_{zz}} \ddot{\psi} + (I_{s_{yy}} - I_{s_{xx}}) \dot{\phi} \dot{\theta} + I_{s_{xz}} \dot{\theta} \dot{\psi} \end{aligned}$$

$$\begin{aligned} &3I_o L_1 \ddot{y} + 3I_o DL_1 \ddot{\phi} + \frac{3L_1}{H} mgy + \frac{3L_1}{H} mgD\phi + \frac{3Z_3 L_1}{H} (y + D\phi) \\ &- (X_1 - X_2) K + (Y_2 - Y_1) F = -I_{s_{xz}} \ddot{\phi} + I_{s_{zz}} \ddot{\psi} + (I_{s_{yy}} - I_{s_{xx}}) \dot{\phi} \dot{\theta} + I_{s_{xz}} \dot{\theta} \dot{\psi} \end{aligned}$$

$$\begin{aligned} (X_2 - X_1) K + (Y_2 - Y_1) F &= -3I_o L_1 \ddot{y} - [3I_o DL_1 + I_{s_{xz}}] \ddot{\phi} + I_{s_{zz}} \ddot{\psi} \\ &- \frac{3L_1}{H} mgy - \frac{3L_1}{H} mgD\phi - \frac{3Z_3 L_1}{H} (y + D\phi) + I_{s_{xz}} \dot{\theta} \dot{\psi} + (I_{s_{yy}} - I_{s_{xx}}) \dot{\phi} \dot{\theta} \end{aligned}$$

In summary, external forces in x, y, z direction can be described as:

Forces in x-axis:

$$\begin{aligned} (X_2 - X_1)K + (Y_2 - Y_1)F = & -3I_o L_1 \ddot{y} - [3I_o DL_1 + I_{xz}] \ddot{\phi} + I_{zz} \ddot{\psi} \\ & - \frac{3L_1}{H} mgy - \frac{3L_1}{H} mgD \phi - \frac{3Z_3 L_1}{H} (y + D \phi) + I_{xz} \dot{\theta} \dot{\psi} + (I_{yy} - I_{xx}) \dot{\phi} \dot{\theta} \end{aligned}$$

Forces in y-axis:

$$\begin{aligned} (Y_1 + Y_2)A = & 3I_o C \ddot{y} + (3I_o CD + 2D^2 m + I_{xx}) \ddot{\phi} - I_{xz} \ddot{\psi} + \frac{3mgC}{H} y + \frac{3mgCD}{H} \phi \\ & + \frac{C}{H} (Z_1 + Z_2 + Z_3) y + \frac{DC}{H} (Z_1 + Z_2 + Z_3) \phi + (I_{zz} - I_{yy}) \dot{\theta} \dot{\psi} - I_{xz} \dot{\phi} \dot{\theta} - (NLa_2 - NLa_1) D \end{aligned}$$

Forces in z-axis:

$$\begin{aligned} Z_1 + Z_2 + Z_3 = & (M_s + 3m) \ddot{z} + 5mL_1 \ddot{\theta} + 3mg + (M_s + 3m) g \cos \theta \cos \theta \\ & + M_s (\dot{\phi} \dot{y} - \dot{\theta} \dot{z}) - NLa_T \end{aligned}$$